Measurement of the $K_{\mu 3}^+$ Decay Parameters

X2 COLLABORATION

D. HAIDT AND J. STEIN
III. Physikalisches Institut der Technischen Hochschule, Aachen, Germany

AND

S. NATALI, G. PISCITELLI, AND F. ROMANO
Istituto di Fisica dell'Università di Bari, Istituto Nazionale di Fisica Nucleare, Sezione di Bari, Italy

AND

E. FETT
Fysisk Institutt, Universitetet i Bergen, Norway

AND

J. LEMONNE,* T. I. PEDERSEN, AND S. N. TOVEY
CERN, Geneva, Switzerland

AND

V. BRISSON AND P. PETIAU
Ecole Polytechnique, Paris, France

AND

C. D. ESVELD AND J. J. M. TIMMERMANS
Fysisch Laboratorium, University of Nijmegen, Nijmegen, Netherlands

AND

B. AUBERT, L. M. CHOUNET, AND LE DONG
Laboratoire de l'Accélérateur Linéaire, Orsay, France

AND

F. BOBISUT, H. HUZITA, AND F. SCONZA
Istituto di Fisica dell'Università di Padova, Istituto Nazionale di Fisica Nucleare, Sezione di Padova, Italy

AND

A. MARZARI-CHIESA AND A. E. WERBROUCK
Istituto di Fisica dell'Università di Torino, Istituto Nazionale di Fisica Nucleare, Sezione di Torino, Italy

(Received 1 June 1970)

A sample of K^+ mesons stopped in the CERN 1.1-m³ heavy-liquid bubble chamber has been used to study the Dalitz-plot density and the μ^+ polarization in $K_{\mu 3}^+$ decay and to measure the $K_{\mu 3}^+$ and K_{e3}^+ branching ratios. All three analyses are described in detail, and they are used, separately and combined, to study the form of the strangeness-changing, semileptonic weak interaction. This is found to be consistent with a coupling of vector currents and to be invariant under time reversal. The vector form factors are studied with a wide range of assumptions as to their possible four-momentum (q^2) dependence, and the results of all three measurements are in agreement. If λ_+ is fixed at 0.029 (the average value from K_{e3}^+ experiments) and if ξ is assumed to be independent of q^2, then the result is $\xi=-0.65\pm0.13$. Assuming that $f_+(q^2)$ and $\xi(q^2)$ are both linear functions of q^2, a three-parameter fit gives $\lambda_+=0.060\pm0.019$, $\xi(0)=-1.0\pm0.5$, and $\xi(5.1m_\pi^2)=-0.97\pm0.20$.

I. INTRODUCTION

THIS experiment is a high-statistical-precision study of the three-body leptonic decays of the K^+ mesons:

$$K_{l3}^+\begin{cases}K_{\mu 3}^+: & K^+\to\pi^0\mu^+\nu\\ K_{e3}^+: & K^+\to\pi^0 e^+\nu.\end{cases}$$

In $K_{\mu 3}^+$ decay, the Dalitz-plot population density and muon polarization have been analyzed, and the absolute decay rate of each mode determined. These properties have been studied previously in a variety of detectors, and the difficulty in interpreting the results in a consistent manner has often been discussed.[1] In order to

[1] See, for example, J. W. Cronin, in *Proceedings of the Fourteenih International Conference on High-Energy Physics, Vienna, 1968*, edited by J. Prentki and J. Steinberger (CERN, Geneva, 1968), p. 281.

* Now at Université Libre de Bruxelles, Belgium.

extract the maximum of information from these decays, the complete track of the charged lepton should be observed, including the decay positron of the μ^+, and both γ rays should be detected and their energies measured. In addition, the γ rays should be unambiguously assigned to the correct origin, and the nature of the charged secondary should be recognizable.

In most detectors these requirements are in conflict with the need to acquire high statistical precision. In particular, the small statistical errors make it important to select the correct events cleanly from the large background of other decay modes. This implies the observation of small-scale phenomena, for instance a π-μ-e decay chain, in a detector large enough to contain the maximum-range muon from $K_{\mu 3}^+$ decay. Further, a high γ-ray conversion efficiency can only be achieved with a dense medium and a corresponding loss of measurement precision. A good compromise was achieved in the large heavy-liquid bubble chamber which was available for this experiment.

A. Theoretical Framework

The study of the properties of the K_{l3} decays bears upon the theories of the weak and the strong interactions. In particular, one can test the dominance of the vector coupling in this decay, its invariance under time reversal, and the ability of different strong-interaction theories to predict the behavior of the hadronic part of the matrix element.

With the basic assumptions that the Langrangian is generated by a local coupling of currents, and that the two-component theory of the neutrino and μ-e universality are valid, the generalized matrix element can be written[2] in the form

$$M=(G/\sqrt{2})\bar{u}_\nu(\mathbf{p}_\nu)(1-\gamma_5)\times\{m_K f_S+\tfrac{1}{2}i[(p_K+p_\pi)_\lambda f_+ +(p_K-p_\pi)_\lambda f_-]\gamma_\lambda +i(f_T/m_K)\sigma_{\lambda\tau}(p_K)_\lambda(p_\pi)_\tau\}u_l(-\mathbf{p}_l),$$

where f_S, $f_\pm$, and f_T are, respectively, the scalar, vector, and tensor form factors which express phenomenologically the contributions of the strong interactions. Any of the form factors may be functions of q^2, the square of the four-momentum transferred to the lepton pair. The limits of q^2 are m_l^2 and $(m_K-m_\pi)^2$; hence in $K_{\mu 3}$ decay the physical region extends from $0.6m_\pi^2$ to $7.1m_\pi^2$.

The invariance of the Hamiltonian for the interaction under time reversal requires that the form factors have the same phase and that the component of lepton polarization perpendicular to the plane of the decay be zero. This polarization has been measured, in this and other experiments,[3] and is compatible with zero. Therefore in most of the following analysis the form factors are taken to be relatively real.

With the aid of the Dirac equation, the matrix element becomes

$$M=(G/\sqrt{2})\bar{u}_\nu(\mathbf{p}_\nu)(1-\gamma_5)\times\tfrac{1}{2}[F_- m_l+iF_+(p_K+p_\pi)_\lambda\gamma_\lambda]u_l(-\mathbf{p}_l),$$

where

$$F_-:=\frac{2m_K f_S}{m_l}+f_-+\frac{f_T}{m_K}\left[m_l+\frac{2p_K\cdot(p_l-p_\nu)}{m_l}\right]$$

and

$$F_+=f_+ +\frac{m_l}{m_K}f_T.$$

All experimental evidence is consistent with a pure vector coupling, and the absence of scalar and tensor terms is reinforced by the results of this experiment (see Sec. IV). In this case $F_\pm$ reduce to $f_\pm$, respectively.

Any property of the K_{l3} decays can be predicted from a knowledge of the form factors. In this experiment measurements were made of the following:

(i) the $K_{\mu 3}^+$ and K_{e3}^+ absolute rates and their ratio,
(ii) the Dalitz-plot density in $K_{\mu 3}^+$,
(iii) the μ^+ polarization in $K_{\mu 3}^+$.

Each of the measurements is used independently to estimate the unknown parameters f_+ and f_-. The three results have been previously published in several letters[4]; here the analysis is presented in greater detail and the results of the three methods are compared and combined.

The form factors $f_\pm(q^2)$ are expanded in the usual manner:

$$f_\pm(q^2)=f_\pm(0)\left(1+\lambda_\pm\frac{q^2}{m_\pi^2}\right).$$

We write their ratio as

$$\xi(q^2)=\frac{f_-(q^2)}{f_+(q^2)}=\xi(0)+\Lambda\frac{q^2}{m_\pi^2}, \qquad (1)$$

where $\Lambda=\xi(0)(\lambda_- -\lambda_+)$ for small λ_+. It was always found that the parameters $\xi(0)$, Λ, and λ_+ used in the linear expansions of $f_\pm(q^2)$ were correlated. However, in each analysis it is possible (see Appendix C) to represent a linear variation of $\xi(q^2)$ by a pair of uncorrelated parameters $\xi(q^2=q_*^2)$ and Λ or, alternatively, $\xi(0)$ and $\xi(q^2=q_*^2)$. The value of q_*^2 depends essentially on the experimental method used to determine ξ, but also on the kinematical cuts which have been made. It is therefore different not only for the three analyses described here, but also it may differ in two experiments both determining, for example, the μ^+ polarization. However, this procedure does not remove the correlations between λ_+ and the other parameters. When the

[2] For the notation, see Appendix A.

[3] M. L. Longo, K. K. Young, and J. A. Helland, Phys. Rev. **181**, 1808 (1969); D. Bartlett, C. E. Friedberg, K. Goulianos, and D. Hutchinson, Phys. Rev. Letters **16**, 282 (1966); **16**, 601 (1966); R. J. Abrams, A. Abashian, R. E. Mischke, B. M. K. Nefkens, J. H. Smith, R. C. Thatcher, L. J. Verhey, and A. Wattenberg, Phys. Rev. **176**, 1603 (1968).

[4] X2 Collaboration: J. Bettels *et al.*, Nuovo Cimento **56A**, 1106 (1968); T. Eichten *et al.*, Phys. Letters **27B**, 586 (1968); D. Haidt *et al.*, *ibid.* **29B**, 691 (1968); **29B**, 696 (1968).

statistics of an experiment permit only a one-parameter fit (constant ξ) then the quantity actually determined is $\tilde{\xi}=\xi(q_*^2)$. It should be remarked that q_*^2 is *not*, in general, the average q^2 value of the events analyzed.

In the present experiment,

(i) the measurement of the $K_{\mu 3}^+/K_{e3}^+$ branching ratio determined $\xi(3.9m_\pi^2)$ as a function of λ_+ (Sec. II);

(ii) in the Dalitz-plot density analysis (Sec. III B) a three-parameter fit was possible using λ_+ and the uncorrelated variables $\xi(0)$ and $\xi(6.8m_\pi^2)$;

(iii) the result from the μ^+ polarization determination (Section III C) is independent of λ_+ and is expressed in terms of the uncorrelated variables $\xi(0)$ and $\xi(4.9m_\pi^2)$.

For the interpretation of the results, it is also useful to decompose the hadronic part of the matrix element into two amplitudes[5] corresponding to spin-parity 1^- and 0^+; these are related to two form factors f_+ and f, respectively, with

$$f=f_+ + \frac{q^2}{(m_K^2-m_\pi^2)} f_- .$$

Keeping only linear terms in the q^2 developments of $f(q^2)$ and $f_+(q^2)$,

$$f(q^2)=f(0)\left(1+\lambda\frac{q^2}{m_\pi^2}\right)$$

and

$$f_+(q^2)=f_+(0)\left(1+\lambda_+\frac{q^2}{m_\pi^2}\right).$$

If $f_-(0)$ is finite, then $f(0)=f_+(0)$ and, apart from normalization, the form factors can be described with only two parameters, which can be taken as (λ,λ_+) or, to be more conventional, as λ_+ and $\xi(0)$, with

$$\xi(0)=(\lambda-\lambda_+)[(m_K^2-m_\pi^2)/m_\pi^2]. \quad (2)$$

The linear development of $f(q^2)$ and $f_+(q^2)$ implies, in fact, that $\lambda_-=0$. The results of all three methods will be also given in this presentation, which will be referred to as the "f,f_+" parametrization.

B. Experimental Conditions

In the present exposure a beam produced in an internal target in the CERN Proton Synchrotron (PS) was brought to rest in the 1.1-m³ heavy-liquid bubble chamber, placed in a magnetic field of 1.9 T and filled with freon C_2F_5Cl (density 1.2 g cm^{-3}, radiation length 25 cm); 4.5×10^6 K^+ mesons were stopped, with an average of seven per picture. The chamber is a cylinder of diameter 110 cm and depth 110 cm and it was arranged that 70% of the K^+ stopped in a zone of about 15 cm radius around the center of the chamber.

[5] T. D. Lee and C. S. Wu, Ann. Rev. Nucl. Sci. 16, 471 (1966).

In order to study the properties of $K_{\mu 3}^+$ decay more fully, completely detected events are required. With the above conditions a large fraction of the muons from $K_{\mu 3}^+$ decay (maximum range 48 cm) stopped in the chamber and their decay positrons were observed. The average conversion probability of a γ ray was 70% and the error on its energy determination, averaged over all dip angles, was about 25%. A measurement of the γ-ray energies is needed only to choose between the two possible π^0 momenta obtained from the kinematical constraint equations when the directions of the γ rays are introduced. The above accuracy is sufficient to select the correct solution in 96% of the cases and the π^0 momentum is known, after fitting, to 6 MeV/c. Thus a sample of about 30 000 completely detected, well-measured $K_{\mu 3}^+$ events are expected.

For the determination of the $K_{\mu 3}^+/K_{e3}^+$ branching ratio, the detection of the decay γ rays was not required, and the identification of the events was based solely on the appearance of the charged secondaries. The highest-energy positron from K_{e3}^+ decay curves in the magnetic field such that its "maximum displacement" from the K^+ decay point is 45 cm for nondipping tracks. As will be described, in the determination of the decay rates and branching ratio, the loss of very high-energy positrons was avoided, either by imposing a very small decay volume for the K^+ or by a potential path cut. A clean sample of $K_{\mu 3}^+$ was obtained using a range cut. The small remaining contaminations, due mainly to in-flight pionic decays, could be accurately estimated; the final π-μ-e decay chain was clearly visible in 60% of the cases when a π^+ came to rest and decayed, and such events were used to determine the contamination.

In all parts of the analysis which follows, the small statistical errors make it important to reduce the systematic errors arising mainly from the backgrounds caused by other decay modes. Unless the nature and effect of a background could be precisely determined, it was removed by restricting the analysis to selected configurations. Such cuts were applied whenever the resulting loss in statistical accuracy was more than compensated for by the reduction of systematic uncertainties. This explains why the samples used are substantially smaller than the number of events available.

II. DETERMINATION OF BRANCHING RATIOS AND DECAY RATES

The branching ratios $K_{\mu 3}^+/K_{e3}^+$, $K_{\mu 3}^+/K_\tau^+$ and K_{e3}^+/K_τ^+ have been determined. The ratio between the leptonic modes is used, under the assumptions of μ-e universality and a vector coupling, to establish a relationship between the parameters λ_+, $\xi(0)$, and Λ. This ratio is given by

$$R(\lambda_+,\xi(0),\Lambda)=\frac{\Gamma(K_{\mu 3})}{\Gamma(K_{e3})}=\int\rho_\mu dE_\pi dE_\mu \Big/ \int\rho_e dE_\pi dE_e ,$$

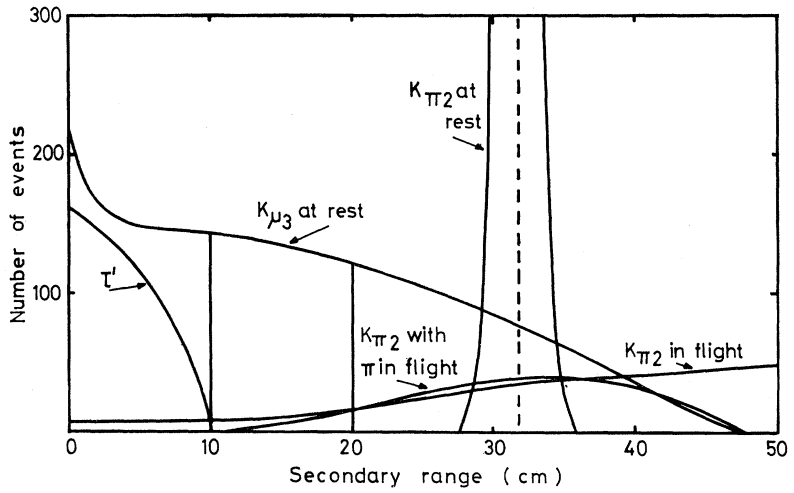

FIG. 1. Estimated background of pionic events as a function of the μ^+ range.

where $\rho_l=\rho(E_\pi,E_l;f_+,f_-)$ is the Dalitz-plot density and the integrals are performed over the respective Dalitz-plot areas. If, in order to avoid backgrounds, only selected parts of the Dalitz plots are used, then a partial branching ratio $R'(\lambda_+,\xi(0),\Lambda)$ may be defined. It should be stressed that no approximation is required when R' is used to determine a relationship between the unknown parameters λ_+, $\xi(0)$, and Λ. Indeed, a given number of events in a background-free region will provide a more accurate determination, due to the smaller systematic errors, than the same number spread over the entire energy interval.

In order to compute total decay rates it is necessary to convert R' into R. This, however, requires a knowledge of the Dalitz-plot density distribution, i.e., of the form factors involved.

A. Experimental Procedure

Two points are essential to the measurements of decay rates: unambiguous event identification and well-known detection efficiencies. In an attempt to meet these requirements, the following method of analysis was adopted in this part of the experiment.

The identification of $K_{\mu 3}$ and K_{e3} events was based solely on the characteristics of the charged secondary. Thus no corrections for γ detection efficiencies are required. A fiducial volume cut for the K-decay points or a potential path cut on secondary tracks assured a 100% geometrical detection efficiency. In these conditions, K_{e3} events are subject to only relatively small backgrounds and no cut on the positron energy spectrum has been applied. Muon (and pion) candidates have been accepted only if their range was between 10 and 20 cm ($152.1\leq E_\mu\leq 178.4$ MeV). This part of the spectrum is expected to be the least contaminated by backgrounds, as is illustrated in Fig. 1. In Fig. 2, the fraction of $K_{\mu 3}$ decays selected is seen to be practically independent of the shape of the muon range spectrum. It amounts to $(29.2\pm 0.3)\%$. The small uncertainty quoted allows for a wide variation of the parameters involved.

1. Event Selection

About 15% of the film was scanned twice for K^+ mesons which, from ionization, appeared to decay at rest into a single charged secondary. The secondary was required to stop into the chamber or otherwise undergo an interaction in flight producing no visible prongs.

The events were classified as follows:

Muon events. The muon event was identified by its decay positron and by the absence of a visible π-μ-e decay chain. It is clear that some pionic decays will fall into this category.

Pion events. The pion was identified by a clearly visible π-μ-e decay chain. These events enable a correction to be made to the background to $K_{\mu 3}$ decay arising from the pionic K-decay modes. They were also used to determine the momentum spectrum of K^+ mesons decaying in flight but erroneously classified as decays at rest.

Both muon and pion events were accepted only if their secondary showed no scatter greater than 20° (measured in projection).

Positron events. The positron was recognized as a track with minimum ionization along its entire length, showing characteristic spiraling, bremsstrahlung, or δ-ray production.

Ambiguous events. In a few cases the secondary could

TABLE I. Numbers of recorded events.

Quantity determined	τ	$K_{\mu 3}$	K_{e3}
Initial sample[a]	12 372	1618	7587
$K_{\mu 3}/\tau$ ratio	11 811	1505	···
K_{e3}/τ ratio	7169	···	4385
$K_{\mu 3}/K_{e3}$ partial ratio	···	1398	6652

[a] After the cuts on muon range and on the lepton dip angle (<45°).

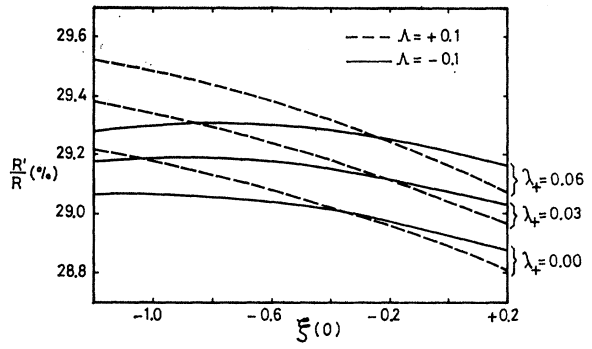

FIG. 2. Percentage of $K_{\mu 3}$ events in the interval $152.1 < E_\mu < 178.4$ MeV as a function of λ_+, $\xi(0)$, and Λ.

not be unambiguously classified. Two types of ambiguity have been distinguished:

(a) There existed a kink on the secondary which could either be attributed to a positron scattering or to the decay of a pion or a muon. After cuts, mainly on dip angle (see next section), only seven such events remained. Of these, two had a track length between 10 and 20 cm to the possible decay point. These events could be neglected in comparison with the total number of events recorded (see Table I).

(b) The secondary disappeared in flight. This could be either due to a positron annihilation or to a π^+ interaction producing no visible prong.

τ decays were noted in addition to the event topologies described above. This decay mode, leading to three charged secondaries of short range, is easily recognized and was used to normalize the K_{l3} decay rates.

2. Geometrical Cuts

After measurement the following cuts were applied to the events.

(a) Events were not accepted if the K^+ had a dip angle greater than 0.8 rad or if the K^+ scattered in the 10 cm prior to its apparent decay point. These cuts greatly reduced the backgrounds or misclassifications due to K^+ decays in flight and to scatterings on the K^+ or on the secondary.

(b) To avoid difficulties of recognition in the case of steeply dipping tracks, only secondaries with dip angle less than 45° were retained for the final analysis.

TABLE II. Corrections to the recorded $K_{\mu 3}$ and K_{e3} samples.

$K_{\mu 3}$ sample		K_{e3} sample	
Type of correction	% correction	Type of correction	% correction
π^+ taken as μ^+ [a]	-7.8 ± 0.8	e^+ annihilation	$+1.9\pm0.2$
$K_{\mu 2}$ (K decay in flight)	-0.5 ± 0.5	τ' decays	-2.3 ± 0.4
$K_{\pi 2}$ (π decay in flight)	-7.6 ± 0.6	$K_{\mu 3}$ decays	-0.5 ± 0.2
$K_{\mu\nu\gamma}$	-2.6 ± 0.5	K_{e5} radiative	-1.0 ± 1.0
Total	-18.5 ± 1.3	Total	-1.8 ± 1.1

[a] $K_{\pi 2}$ and τ' with K decay in flight, $K_{\pi\pi\gamma}$, and $K_{\pi 2}$ at rest with a π scatter.

(c) In order to determine the $K_{\mu 3}^+/K_\tau^+$ and K_{e3}^+/K_τ^+ ratios, fiducial volume cuts, ensuring 100% geometrical detection efficiencies, were applied to the K^+ decay points. The distance from the K^+ decay point to the chamber wall was required to be greater than 45 cm for positron secondaries and 25 cm for muon secondaries. This latter value followed from the already mentioned range cut on pion and muon secondaries ($10.0 \leq$ range < 20.0 cm). For the measurement of the $K_{\mu 3}^+/K_{e3}^+$ branching ratio, a potential path cut was applied to the charged secondary, muon as well as positron. More specifically, a secondary track has been retained only if the entire track of the highest-energy positron from K_{e3}^+ decay at rest, produced at the same point and in the same direction, would have been inside the visible volume of the chamber. Furthermore, this hypothetical positron was assumed to lose its energy by ionization only.

After double scan and after cuts, each event category had a scanning efficiency greater than 99%. The numbers of events, before and after the fiducial volume and potential path cuts described above, are recorded in Table I.

3. Corrections

Table II summarizes the various corrections which were applied to our $K_{\mu 3}$ and K_{e3} samples. These were estimated in the following manner.

a. $K_{\mu 3}$ sample. The muon emitted when a π^+ comes to rest in C_2F_5Cl is not always observed, as its range is only 1.7 mm, and so a stopping π^+ may be frequently mistaken for a μ^+. Most of the pionic background is removed by the requirement that the muon range should be between 10 and 20 cm (Fig. 1). However, there remains a background from rare or "in-flight" pionic decays; these are enumerated below. A small source of background is due to $K_{\mu 2}$ decays in flight and to radiative $K_{\mu 2}$ decays ($K_{\mu\nu\gamma}$). The corrections were determined as follows:

(i) Stopping π^+. To correct for the contribution from stopping π^+ with no subsequent visible π-μ-e decay chain, use was made of the recorded pion events with a range between 10 and 20 cm and a visible decay chain. Such events are due to radiative decay ($K_{\pi\pi\gamma}$), to $K_{\pi 2}$ and τ' events in which the K^+ decayed in flight, and to $K_{\pi 2}$ decays with a small scatter on the π^+. The probability of observing a π-μ-e decay chain has been determined using pion secondaries from $K_{\pi 2}$ and τ decays at rest; it was found to be $(60\pm2)\%$. The contribution of such backgrounds to the selected muon sample was estimated to be $(7.8\pm0.8)\%$.

(ii) π^+ decays in flight. The magnitude of the background arising from $K_{\pi 2}$ decay at rest with the π decaying in flight was obtained from a Monte Carlo calculation. The number of $K_{\pi 2}$ events generated was normalized from the number of τ decays observed.

Taking the events with a total track length between 10 and 20 cm and with a projected angle between pion and muon less than 20°, the correction is (7.6±0.6)%.

(iii) K^+ muonic decays in flight. The muon from $K_{\mu 2}$ decay in flight can have a range less than 20 cm if the K^+ decays with a momentum greater than 218 MeV/c. In order to correct for such decays, the momentum spectrum of K decays in flight which appear to occur at rest has to be known. This spectrum was determined experimentally from the kinematics of $K_{\pi 2}$ decays in flight. In Fig. 3 the events with secondaries identified as pions are displayed in a scatter diagram. The range of the pion is plotted versus the cosine of its laboratory emission angle with respect to the kaon; curves correspond to lines of constant K momentum. $K_{\pi 2}$ decay in flight of momentum less than 300 MeV/c can only populate the lower part of the diagram, while τ' decays in flight can only contribute to the upper part. Events arising from the $K_{\pi\pi\gamma}$ mode and from $K_{\pi 2}$ decays at rest with a π^+ scatter will be distributed isotropically in angle. Subtracting such events, the contribution from $K_{\pi 2}$ decays in flight can be estimated. Correcting for the fact that only secondaries with a range between 10 and 20 cm were selected and taking into account the π-μ-e visibility, the K-momentum spectrum shown in Fig. 4 is obtained. The fraction of $K_{\mu 3}$ decays in flight in our sample of "at-rest" decays is (2.0±0.5)%. The corresponding contribution of $K_{\mu 2}$ decays in flight to the $K_{\mu 3}$ sample is (0.5±0.5)%.

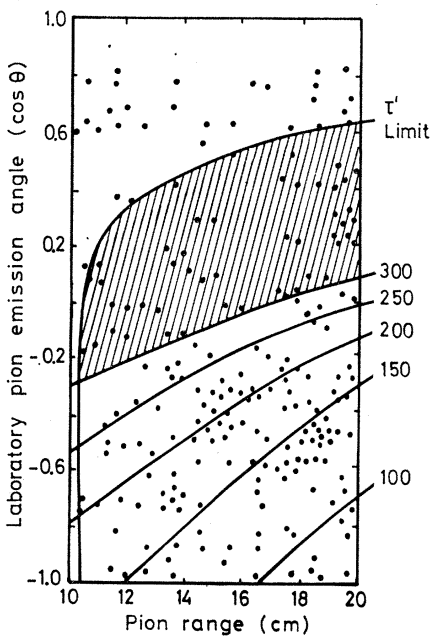

FIG. 3. Scatter diagram of events with secondaries identified as pions; the lines in the lower half of the plot refer to $K_{\pi 2}$ decays with the indicated K^+ momenta. The curve "τ' limit" is the line above which all secondaries from τ' decay in flight must lie, calculated for all K^+ momenta up to 300 MeV/c.

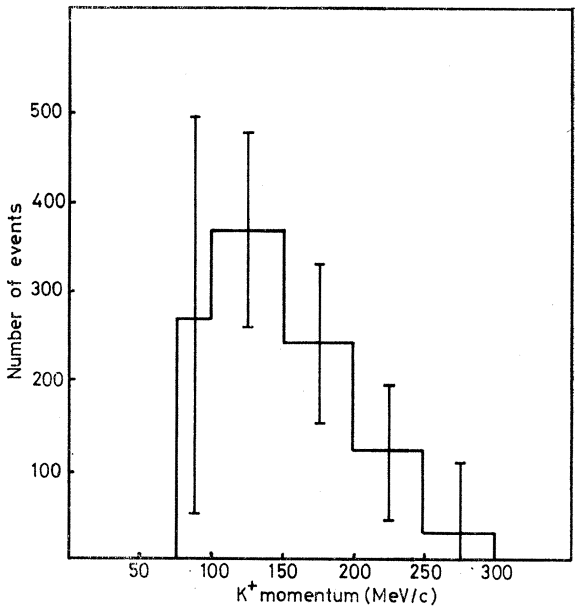

FIG. 4. Momentum spectrum of K^+ decays in flight which appear to be at rest.

(iv) Radiative $K_{\mu 2}$ decays. The background from $K_{\mu\nu\gamma}$ was estimated to be (2.6±0.5)%. The uncertainty is due to a lack of knowledge as to how much "structure terms" and inner bremsstrahlung contribute to the decay rate.[6]

b. K_{e3} sample. Corrections were applied for positron annihilations in flight, for τ' and $K_{\mu 3}$ decays with short undetectable secondaries, and for radiative K_{e3} decays.

(i) e^+ annihilation. Secondaries disappearing in flight without producing visible prongs can be interpreted either as positrons or pions. For those events showing no characteristic positron signature, a search has been made for γ rays pointing to the annihilation point. In Fig. 5 the distribution of the cosine of the angle of emission of the γ rays with respect to the interacting secondary is shown. The distribution is peaked significantly in the forward direction. The flat tail is due to the decay γ rays from π^0's produced in π^+ charge-exchange reactions, while the peak is identified as arising from positron annihilations in flight. Taking account of the events without a visible γ ray and of the scanning efficiency, which for this type of event is only (84±5)% after double scan, the correction becomes (1.9±0.2)%.

(ii) $K_{\mu 2}$ decays with an undetected μ^+-e^+ transition. Such events could be confused with a K_{e3} decay if the decay positron of the muon is collinear with the direction of the stopping muon and if the ionization change is not seen. The very small number of ambiguous events with a visible kink allows us to neglect this background.

[6] D. E. Neville, Phys. Rev. 124, 2037 (1961); only inner bremsstrahlung terms have been taken.

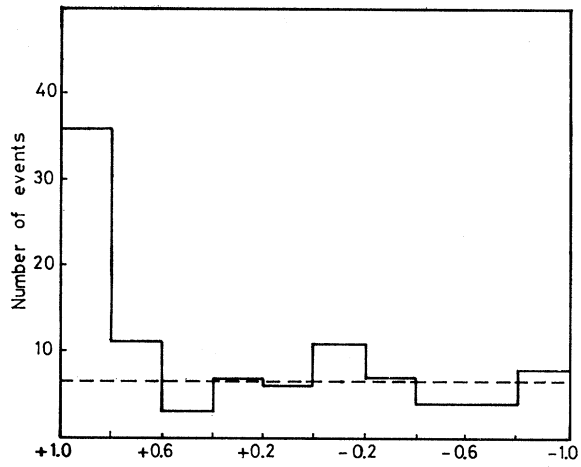

FIG. 5. Distribution of the cosine of the emission angle of γ rays associated with secondaries disappearing in flight.

(iii) τ' and $K_{\mu 3}$ decays. These decays can be mistakenly classified as a K_{e3} decay. For τ' events this occurs in the following cases:

(1) the π^+ is very short and not seen, and the μ^+-e^+ transition is not detected;

(2) the π^+ is long enough, but the π^+-μ^+ and μ^+-e^+ decays are collinear and mistaken for a fluctuation in ionization;

(3) the π^+ is emitted in the direction of the stopping K^+ with an energy such that the change in ionization is too small to allow the observation of the K^+-π^+ transition. Furthermore, the μ^+-e^+ decay has to be unseen.

By a careful study of similar π^+ configuration in τ decay, the proportion of such events in τ' decays is found to be $(6.6\pm0.8)\%$, and the contamination in the K_{e3} sample is then computed to be $(2.3\pm0.4)\%$.

For $K_{\mu 3}$ decays, the background is due to the same type of events, but with the π^+ replaced by a μ^+, and without the constraint on the π^+-μ^+-e^+ chain which does not exist. We have thus to determine the probability that the μ^+-e^+ transition is not seen as a function of the μ^+ energy. This probability is obviously very close to unity for ranges smaller than 1 mm and has been estimated as $(20\pm10)\%$ for a μ^+ from π^+ decay, i.e., having a 1.7-mm range. Weighting the $K_{\mu 3}$ energy spectrum with these probabilities, we obtain that $(0.8\pm0.2)\%$ of the $K_{\mu 3}$ decays can be confused with K_{e3}, which gives a $(-0.5\pm0.2)\%$ correction on the K_{e3} sample.

(iv) Radiative K_{e3}. The correction was based on theoretical calculations by Ginsberg[7] with f_+ assumed to be constant. Weighting with the Dalitz-plot density and integrating over the whole Dalitz plot gives a small correction to the total K_{e3} decay rate: $-(1\pm1)\%$. An error of 100% was assigned to take account of the uncertainties in the calculation.

[7] E. S. Ginsberg, Phys. Rev. 142, 1035 (1966).

Since the $K_{\mu 3}$, K_{e3}, and τ rates are measured relative to each other, they need no correction for decays in flight apart from the fact that only a fraction of the muon spectrum has been observed; the correction for this is negligible.

B. Results

After background subtractions, the partial branching ratio defined as $R'=\Gamma(K_{\mu 3};\ 152.1\leq E_\mu<178.4\ \text{MeV})/\Gamma(K_{e3})$ is found to be

$$R'=0.174\pm0.007.$$

The error contains the statistical error (0.006) and the uncertainties in the corrections (0.004). As mentioned above, R' can be used to establish a relationship between λ_+, $\xi(0)$, and Λ. Figure 6 shows the variation of $\xi(0)$ with Λ for different values of R' with λ_+ fixed exactly at its present "world-average" value for K^+ data of 0.029.[8] In the region of our experimental value, the relationship between $\xi(0)$ and Λ is, to a good approximation, linear:

$$\xi(0)\simeq a(\lambda_+,R')+b\Lambda.$$

Substituting this relationship into Eq. (1), we find that there is a value of q^2 at which $\xi(q^2)$ can be determined independently of the slope Λ:

$$\xi(-bm_\pi{}^2)=a(\lambda_+,R').$$

We find $b=-3.9$ and the result is

$$\xi(3.9m_\pi{}^2)=-0.72\pm0.21 \quad \text{for} \quad \lambda_+\equiv0.029.$$

The value b remains unaffected when λ_+ is varied over reasonable limits and so the most general statement of our result is to plot the function $a(\lambda_+,R')=\xi(3.9m_\pi{}^2)$ for the experimentally determined value of R' and for

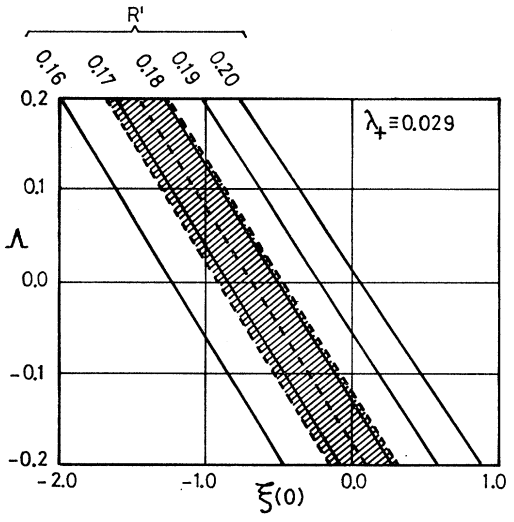

FIG. 6. $R'(\xi(0),\Lambda)$ for $\lambda_+\equiv0.029$; the shaded area represents our experimental result.

[8] C. Rubbia, in Proceedings of the Topical Conference on Weak Interactions, CERN, 1969, p. 227 [CERN Report No. 69-7 (unpublished)].

various λ_+; this is shown in Fig. 7. There is a second solution at $\xi \approx -6.5$ which is rejected by the polarization and Dalitz-plot data.

Our branching ratio measurement can also be interpreted assuming $\lambda_-=0$, and Fig. 8 shows the result in terms of λ_+ and $\xi(0)$.

From R' the total $K_{\mu 3}/K_{e3}$ branching ratio R can be calculated making use of Fig. 2; it is

$$R=0.596\pm0.025,$$

where the error includes an uncertainty in the ratio of R' to R: $(29.2\pm0.3)\%$.

The individual leptonic branching ratios have been determined:

$$\Gamma(K_{\mu 3})/\Gamma(\tau)=0.503\pm0.019,$$
$$\Gamma(K_{e3})/\Gamma(\tau)=0.850\pm0.019.$$

Taking the τ^+ branching ratio to be $(5.57\pm0.04)\%$ of all K^+ decays,[9] we determine the branching ratios of each leptonic mode relative to all decays to be

$$\Gamma(K_{\mu 3})/\Gamma(\text{all})=2.80\pm0.11\%,$$
$$\Gamma(K_{e3})/\Gamma(\text{all})=4.73\pm0.11\%.$$

Alternatively, using the τ^+ partial decay rate[9] of $(4.51\pm0.03)\times10^6$ sec^{-1}, the partial K_{l3}^+ decay rates are

$$\Gamma(K_{\mu 3}^+)=(2.27\pm0.09)\times10^6 \text{ sec}^{-1},$$
$$\Gamma(K_{e3}^+)=(3.83\pm0.09)\times10^6 \text{ sec}^{-1}.$$

III. $K_{\mu 3}^+$ ANALYSIS

Besides the measurement of the branching ratio $K_{\mu 3}/K_{e3}$, we have carried out two further investigations of the $K_{\mu 3}$ form factors by studying, for $K_{\mu 3}$ decays,

(1) the density of population of the Dalitz plot, and
(2) the polarization of the muon.

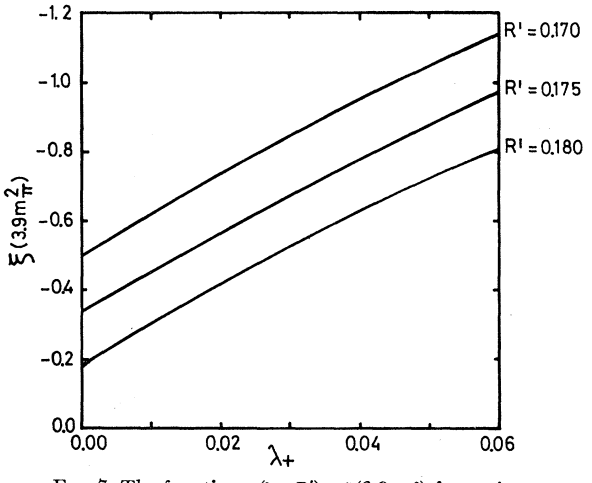

FIG. 7. The function $a(\lambda_+,R')=\xi(3.9m_\pi^2)$ for various values of λ_+ and R'.

[9] Particle Data Group, Rev. Mod. Phys. 41, 109 (1969).

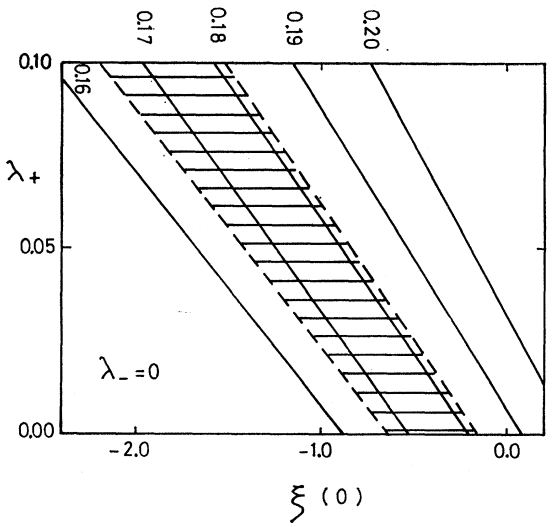

FIG. 8. $R'(\xi(0),\lambda_+)$ for $\lambda_-=0$; the shaded area represents our experimental result.

These analyses require that the kinematics of the decay are well known, which is only possible for complete $K_{\mu 3}$ events in which the μ^+ stops inside the chamber and the two γ rays from the π^0 are visible. With our experimental condition, 25% of the $K_{\mu 3}$ decays present satisfy the above criteria.

In Sec. III A, we describe the procedure used to obtain a pure sample of fully reconstructed $K_{\mu 3}$ events. Sections III B and III C are devoted to the studies of the Dalitz-plot density and of the muon polarization, respectively, under the assumption of a pure vector interaction. The possible contribution of scalar or tensor terms is considered in the next part of the paper.

A. Selection of Events

All the available pictures ($\sim6\times10^5$) were scanned for K^+ decay at rest in the mode $K^+\to\pi^0\mu^+\nu$ ($K_{\mu 3}$). A decay is classified as a $K_{\mu 3}$ candidate if it satisfies the following criteria:

(1) There are two measurable γ rays pointing unambiguously to a common K^+ vertex on all three views;
(2) the ionization of the K^+ track is consistent with a stopping particle;
(3) the charged secondary undergoes no scattering with a projected angle greater than 20°, stops in the chamber, and decays into a positron visible along its entire length.

To ensure a good visibility of events, the K^+ stopping point was required to lie in a fiducial volume in the central region of the chamber defined as follows[10]:

$$r_K<47 \text{ cm}, \quad -80<z_K<-30 \text{ cm}.$$

The dip angle of the K^+ track had to be less than 45° so that the ionization could be well observed and the

[10] The coordinate system used is described in Appendix A.

contamination of K^+ decays in flight reduced. The μ^+ dip angle had also to be less than 72° so as to ensure good measurement conditions and muon-positron distinction. The scanning efficiency was determined by a partial rescanning (60% of the available film) to be 61% for the first scan and 73% for the second scan.

The retained events were measured and processed through a chain of programs for geometrical reconstruction and kinematical fitting. The directions of all tracks are well known; typical errors on dip and azimuthal angles are of the order of 30 mrad. The range of the stopping muon is determined with 2% precision and the momentum is deduced with an error, mainly due to straggling, of 3%. The momenta of γ rays and μ-decay positrons are determined from curvature following the Behr-Mittner method[11]; hence these measurements are affected by large errors ($\sim$25% for γ rays) due to fluctuations caused by multiple scattering and bremsstrahlung.

Assuming the K^+ to be at rest, using all measured quantities (momenta and directions of the μ^+ and of the two γ rays) and including the π^0 constraint, a two-constraint (2C) fit has been applied to the $K_{\mu 3}$ candidates. Apart from the γ-ray momenta, the values of the variables are not much displaced by the fit due to their relatively small measurement errors. If one assumes p_γ to be unknown and considers the well-measured quantities as fixed, one is left with a zero-constraint fit. This generally leads to two solutions for the π^0 and γ-ray momenta. A correct discrimination between the higher- and lower-energy γ rays is sufficient for the precise determination of the kinematics of a particular $K_{\mu 3}$ event. Errors on the fitted π^0 momenta, taking into account the 3% error on the μ^+ momentum, are around 6 MeV/c.

Even for a pure sample of $K_{\mu 3}$ events, the results may be biased by the kinematical reconstruction when

(1) the choice between the two solutions is wrong,
(2) the association of the γ ray to a K^+ decay point is incorrect.

The first possibility may occur for badly measured γ rays. The second may be due to the presence of ambiguous origins or spurious γ rays. To reduce these biases, a first selection of events was made with the following criteria:

(1) The χ^2 of the $K_{\mu 3}$ (2C) fit was required to be less than 6,[12] and the invariant mass of the two γ rays had to fall in the interval 45–225 MeV (this corresponds to 3 standard deviations from the central value of 135 MeV). These cuts eliminated 8% of all events, many of which were badly measured.

(2) The conversion distance was required to lie between 1 and 50 cm; this rejected 17% of the events. The lower limit is necessary for a good determination of the γ-ray direction, and the upper limit reduces the contamination of spurious γ rays.

The frequency of the choice of the wrong kinematical solution was estimated by Monte Carlo methods to be of the order of 4%. These events do not significantly affect our final results.

An examination of $K\mu_3$ events with a third pointing γ ray showed that as many as 11% of the 2γ-$K_{\mu 3}$ candidates might contain a spurious γ ray. Only 50% of these wrong γ rays still appear to be pointing after measurement. Monte Carlo calculations, which generated spurious γ rays from various sources, show that 20% of these give a $K_{\mu 3}$ fit. Hence the background of such events is at most 1%. Such events could be particularly disturbing in the Dalitz-plot density analysis, but the cuts introduced for the purpose of this study further reduce the background to 0.3% so that no significant influence of these events on the results is expected.

It is equally important to check that the $K_{\mu 3}$ sample is free from background due to other decay modes. The major source of background comes from the modes $K_{\pi 2}$ and τ' with K^+ and π^+ decay at rest, where the π^+ has no visible π-μ-e decay chain; this characteristic decay configuration was only visible on about 60% of stopping π^+. However, these backgrounds affect only limited intervals of the μ^+ range spectrum, since the π^+ range is 31.75 cm in $K_{\pi 2}$ decay and less than 10.4 cm for τ' decay. Therefore, events with μ^+ range L_μ falling either in the zone $L_\mu < 10.4$ cm or around the $K_{\pi 2}$ value ($29.5 < L_\mu < 34$ cm) were discarded. This important cut left 10 900 events, and the selected region of the Dalitz plot is defined by

$$152.7 \text{ MeV} < E_\mu < 199.0 \text{ MeV},$$
$$211.7 \text{ MeV} < E_\mu.$$

These events were fitted to the $K_{\pi 2}$ hypothesis, and rejected when the χ^2 probability of this fit was greater than 0.1%. After all these cuts, the contamination due to $K_{\pi 2}$ and τ' decays at rest is negligible.

The remaining sources of background are

(i) $K_{\mu 3}$ and $K_{\pi 2}$ decays with K^+ decay in flight, and
(ii) $K_{\pi 2}$ with K^+ decay at rest and the π^+ decaying in flight with a (π^+,μ^+) angle less than 20°.

For $K_{\mu 3}$ and $K_{\pi 2}$ decays with K^+ decay in flight, the probabilities to fit the $K_{\mu 3}$ at-rest hypothesis are 40% and 15%, respectively. The K^+ momentum was taken to extend up to 250 MeV/c as indicated by the results of the $K_{\mu 3}/K_{e 3}$ branching-ratio study (see Sec. II), and by the K^+ momentum distribution of events fitting only the $K_{\pi 2}$ decay-in-flight hypothesis. In the regions of the Dalitz plot finally selected for muon polarization or Dalitz-plot density analysis, the contribution of $K_{\mu 3}$

[11] L. Behr and P. Mittner, in Proceedings of the Informal Meeting on Geometry Programs for Heavy-Liquid Bubble Chambers [CERN Report No. 63-23, 1963 (unpublished)].

[12] In several groups this cut was made using the difference between the measured γ-ray energies and their values calculated from the 0C fits.

and $K_{\mu 2}$ decays in flight are estimated to be of the order of 1% and 0.3%, respectively.

For a $K_{\pi 2}$ with K^+ decaying at rest and π^+ decaying in flight with a (π^+, μ^+) angle less than 20°, the probability to fit the $K_{\mu 3}$ hypothesis is high (84%), but these events are localized in a region of the Dalitz plot corresponding to a (π^0,μ^+) angle of the order of 180°. But it will be seen that for the purpose of the polarization analysis we require that $|\hat{p}_\pi \cdot \hat{p}_\mu| < 0.97$; with this cut the contamination is lowered to 0.25% of the $K_{\mu 3}$ events. In the Dalitz-plot density analysis, an even more strict cut is applied, imposing $155 < E_\mu < 197$ MeV and $155 < E_\pi \sim 235$ MeV, so that in this case the background due to such decays is reduced to less than 0.1%.

B. Dalitz-Plot Density

1. General Considerations

a. Analytic expression for density. The partial decay rate of a K^+ into a π^0 with total energy between E_π and $E_\pi + dE_\pi$, and a μ^+ with total energy between E_μ and $E_\mu + dE_\mu$, is proportional to the function $\rho(E_\pi, E_\mu; \xi, \lambda_+) dE_\pi dE_\mu$ which is defined in Appendix B.

If the q^2 dependence of the form factors can be neglected, then

(i) lines of equal population density are parts of hyperbolas; these are shown in Fig. 9 for two values of ξ;

(ii) the π^0 spectra at fixed μ^+ energies are linearly increasing functions of E_π;

(iii) the muon spectra at fixed π^0 energies are parts of parabolas.

The first two statements are slightly modified if a slow q^2 dependence of the form factors is introduced, since q^2 is related to E_π by

$$q^2 = m_K^2 + m_\pi^2 - 2 m_K E_\pi .$$

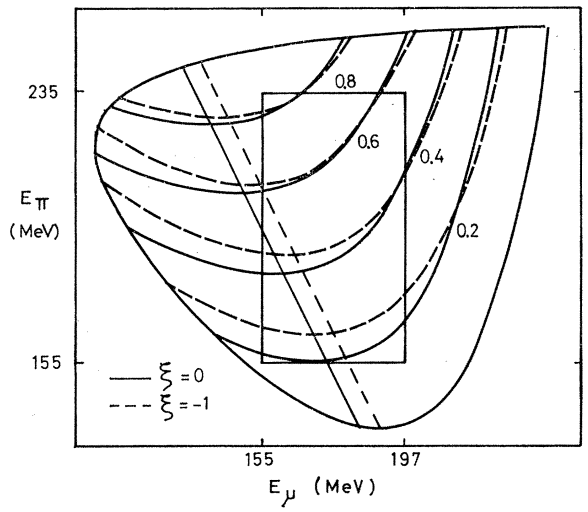

FIG. 9. Curves of equal Dalitz-plot density for $\xi = 0$ and $\xi = -1$. The oblique straight lines show the position of the top of the muon spectra. The analysis has been confirmed to events within the rectangle shown.

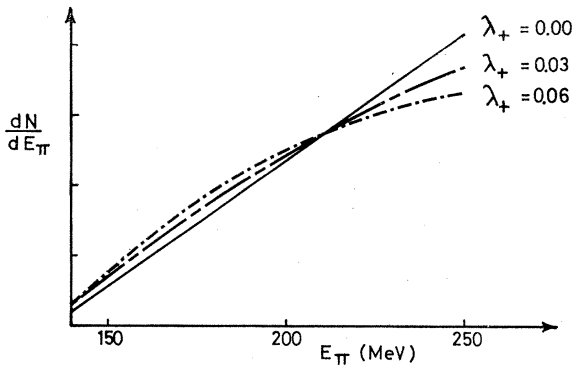

FIG. 10. Modification to the π^0 spectrum at $E_\mu = 180$ MeV (assuming $\xi = -1$) when small λ_+ values are included.

For example, Fig. 10 shows the alteration to the theoretical π^0 spectrum when small values of λ_+ are included.

b. Problem of parasitic solution. If the analysis were restricted to the study of the π^0 spectra at fixed μ^+ energies, each spectrum after normalization would depend on one parameter only (its slope), which is a quadratic function of ξ. Thus a parasitic solution is present, and Fig. 11 shows that this false value of ξ depends only weakly on the μ^+ energy. This suggests that the parasitic solution may appear even in an analysis of the π^0 spectra at several muon energies.

However, each parabolic μ^+ spectrum at a fixed π^0 energy depends on two parameters after normalization, and thus two different values of ξ never lead to the same spectrum. For example, the position $(E_\mu)_{\max}$ of the top of the parabola is a linear function of ξ:

$$(E_\mu)_{\max} = \tfrac{1}{2}(m_K - E_\pi) + \tfrac{1}{4}(m_\mu^2/m_K)(1-\xi) .$$

Therefore the analysis of the μ^+ spectra at fixed π^0 energies yields a unique value of ξ. Unfortunately, the μ^+ energy spectrum is less sensitive to a variation of ξ than the π^0 energy spectrum, but it is reasonable to expect that in the complete analysis of the density the parasitic solution will appear as significantly less likely.

c. Precision of determination of ξ. If a total number of N events has been found in the complete area of the Dalitz plot, it is useful to study how the distribution of these events through the Dalitz plot is modified when ξ is changed. The number ΔN of events falling inside a small area $\Delta S = \Delta E_\pi \, \Delta E_\mu$ of the Dalitz plot is given by

$$\Delta N = N \frac{\rho(E_\pi, E_\mu) \Delta E_\pi \Delta E_\mu}{\int \rho(E_\pi, E_\mu) dE_\pi dE_\mu} ,$$

where the integral is taken over the complete Dalitz plot.

The sensitivity of the various parts of the Dalitz plot in the determination of ξ can be illustrated by computing for each elementary area ΔS, the quantity $\delta\xi$ which will produce a change in ΔN equal to the

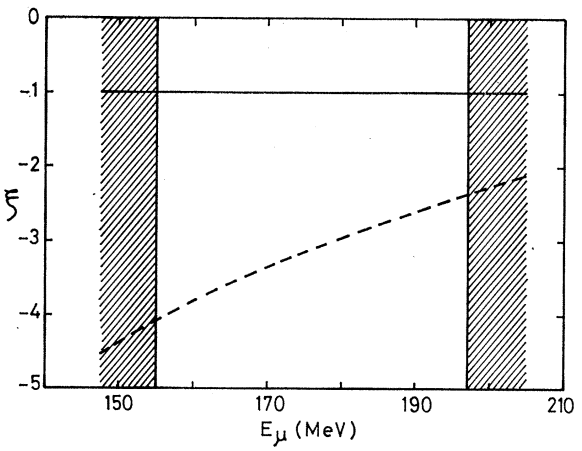

FIG. 11. Assuming $\xi=-1$, then an analysis of the π^0 spectrum at various fixed muon energies yields both the correct solution (solid line) and a parasitic solution (dashed line) whose ξ value varies slowly with the muon energy.

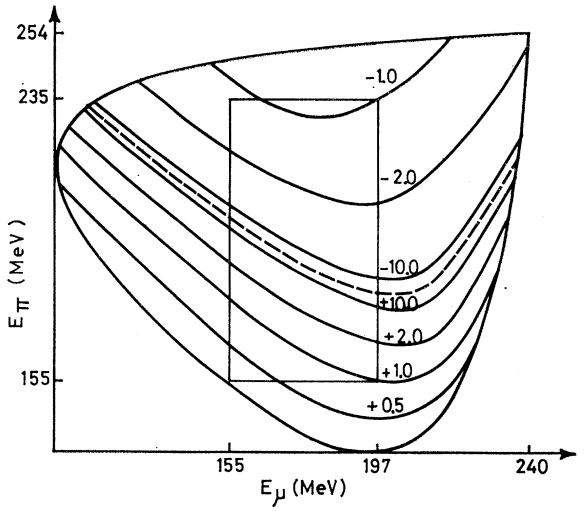

FIG. 12. Sensitivity for ξ determination of various regions of the Dalitz plot (see text); a low value of $|\delta\xi|$ indicates an accurate determination.

statistical uncertainty on ΔN:

$$\frac{\partial(\Delta N)}{\partial\xi}\delta\xi=\sqrt{\Delta N}.$$

The values of $\delta\xi$ have been calculated assuming $N=10^4$ and $\xi=-1$ and looking for the number ΔN of events falling inside small areas $\Delta S=10\times10$ MeV^2 throughout the Dalitz plot. Figure 12 shows lines of equal values of $\delta\xi$; despite its small population, the low-E_π region of the plot appears to be the most sensitive in the determination of ξ.

2. *Determination of Detection Efficiency*

Having selected a sample of events free from background, we need to know the probability to observe each event detected in the chamber, which may be written as

$$P=\frac{\rho(E_\pi,E_\mu;\,\xi,\lambda_+)\times R(E_\pi,E_{\gamma1})\times D(E_{\gamma1})\times D(E_{\gamma2})\times\epsilon(E_\mu)}{\int\int_{(s)}\rho(E_\pi,E_\mu;\,\xi,\lambda_+)\times\epsilon(E_\mu)\left[\int_{(s')}R(E_\pi,E_{\gamma1})\times D(E_{\gamma1})\times D(E_{\gamma2})dE_{\gamma1}\right]dE_\pi dE_\mu}. \tag{3}$$

In this expression,

(i) $\rho(E_\pi,E_\mu;\,\xi,\lambda_+)$ is the $K_{\mu3}^+$ Dalitz-plot density.

(ii) $R(E_\pi,E_{\gamma1})dE_{\gamma1}$ is the probability for a π^0 of energy E_π to decay into two γ rays of energies $E_{\gamma1}$ (within $dE_{\gamma1}$) and $E_{\gamma2}=E_\pi-E_{\gamma1}$. Its form is independent of E_γ (uniform spectrum) and can be written after normalization as

$$R(E_\pi,E_{\gamma1})dE_{\gamma1}=dE_{\gamma1}/p_\pi,$$

where p_π is the π^0 momentum.

(iii) $D(E_{\gamma1})$, $D(E_{\gamma2})$, and $\epsilon(E_\mu)$ are, respectively, the probability to observe in the chamber γ rays of energy $E_{\gamma1}$, $E_{\gamma2}$, and a muon of energy E_μ.

(iv) The total normalization is such that (s) is the useful area of the Dalitz plot and (s') is the possible range of energy for a γ coming from a π^0 with energy E_π; if there is no cut on the γ-ray energy, then

$$\tfrac{1}{2}(E_\pi-p_\pi)<E_\gamma<\tfrac{1}{2}(E_\pi+p_\pi).$$

This expression of the probability density of an event will be used further to construct the likelihood function. Several remarks can be made about the form of the expression written above:

(1) The probability of observing the muon and both γ rays will be correctly written as $\epsilon(E_\mu)\times D(E_{\gamma1})\times D(E_{\gamma2})$ only if no correlation exists in the detection of these particles.

(2) Owing to the manner of normalization, it is clear that the detection efficiencies $D(E_\gamma)$ and $\epsilon(E_\mu)$ need only to be known within a factor.

In the expression for the probability (3), the integral

$$\int_{(s')}R(E_\pi,E_{\gamma1})D(E_{\gamma1})D(E_{\gamma2})dE_{\gamma1}$$

represents the detection probability of a π^0 of energy E_π. Consequently, the denominator of (3) can be rewritten as

$$\int\int_{(s)}\rho(E_\pi,E_\mu;\,\xi,\lambda_+)\epsilon(E_\mu)\epsilon'(E_\pi)dE_\pi dE_\mu.$$

a. Muon detection probability $\epsilon(E_\mu)$. We have defined a sample of events for which the geometrical detection probability of the muon is unity, i.e., for which all muons stop inside the useful volume of the chamber.

This was achieved by simultaneously defining a smaller fiducial volume for K^+ decays and cutting the upper part of the μ^+ spectrum; the K^+ decay volume is a cylinder of radius 30 cm and height 40 cm, and the maximum muon energy is 197 MeV, corresponding to a range of 28.0 cm. These values were chosen so as to maximize the number of remaining events (4642). The muon scanning efficiency was found to be independent of the length of the muon. Furthermore, this fiducial volume cut provides an average potential path for γ-ray conversion which is independent of the energy of the muon.

b. γ-ray detection efficiency $D(E_\gamma)$. The γ-ray detection efficiency depends upon the materialization probability, the scanning efficiency, and the measurability of the electron-positron pair. Several methods can be used to determine the over-all detection efficiency:

(i) For the $K_{\mu 3}$ events, the angular distribution of the γ rays in the π^0 rest frame must be isotropic at all π^0 energies. This property enables an unnormalized γ-ray detection probability to be estimated, but it is not very sensitive and was used only as a check upon the other methods.

(ii) A sample of 6400 $K_{\pi 2}$ decays with one or two γ rays has been measured and fitted. In these events the monoenergetic π^0 produces γ rays with a uniform energy spectrum and the relative γ-ray detection probability is given directly by the shape of this spectrum, which is shown in Fig. 13. However, it is not certain that the losses are identical for these events and for the $K_{\mu 3}$ sample.

(iii) On the $K_{\mu 3}$ events themselves, additional information can be used, namely, the conversion-length distribution of γ rays of a given energy. This method proves to be the most satisfactory and its results will be used in the further analysis. For each energy interval, the total number of γ rays produced is

$$N_T(E_\gamma)=\int_0^\infty n_0 e^{-\mu(E_\gamma)l}dl,$$

where E_γ is the average energy in the interval, $\mu(E_\gamma)$ is the reciprocal of the theoretical materialization length, and n_0 is a normalization coefficient. If $N_s(E_\gamma)$ is the number of observed γ rays in the energy interval, then the γ-ray detection probability is

$$D(E_\gamma)=N_s(E_\gamma)/N_T(E_\gamma). \quad (4)$$

(This provides an absolute value of the over-all detection efficiency, whereas the other methods discussed gave only relative values.)

In order to compute $N_T(E_\gamma)$, the normalization coefficient n_0 is calculated from the number of observed γ-rays with a conversion length between 1 and 10 cm, with a small correction for the losses which are present even at such short distances. This correction was found using the sample of $K_{\pi 2}$ events described above, making the assumption that the $K_{\mu 3}$ sample is subject to the same small losses. Averaged over γ-ray energy, the correction amounted to 3% due to unmeasurable γ rays and 1% due to scanning loss. The latter figure was obtained from the $K_{\pi 2}$ events with one recorded γ ray by predicting the direction of the second γ ray from the kinematical constraint and then making a special search for this γ ray. For the energy range retained in the final $K_{\mu 3}$ analysis, 50 to 195 MeV, a linear correction to n_0 was applied, decreasing from 6% at low energies to 1% at high energies. The absolute γ-ray detection probability $D(E_\gamma)$, deduced from Eq. (4) by this method, is shown in Fig. 14.

For the retained energy interval, $50<E_\gamma<195$ MeV, a straight line, $D(E_\gamma)=D(0)(1+\beta E_\gamma)$, fits the data well, with $\beta=(2.3\pm0.6)$ GeV^{-1}. The parameter $D(0)$ does not enter the analysis as only the relative detection efficiency is needed.

As a check, the conversion length method has also been applied to the sample of $K_{\pi 2}$ events described above in point (ii). The results appear in Fig. 13 and should be compared with the relative γ-ray detection probability derived from the energy spectrum of the same γ rays. Both methods agree except for low values of γ-ray energy ($20<E_\gamma<40$ MeV). Although the observed discrepancy could be explained by a statistical fluctuation or by a loss of events with only one converted low-energy γ ray, it has been decided, for safety, to discard all events having a γ ray with an energy less than 50 MeV. A consequence of this cut is that the maximum γ-ray energy in the $K_{\mu 3}$ sample is 195 MeV.

The π^0 detection efficiency $\epsilon'(E_\pi)$ has been computed, integrating the function $D(E_\gamma)$ shown in Fig. 14 over

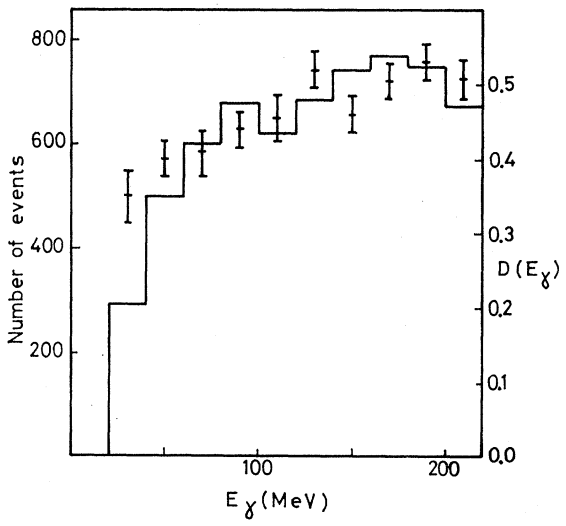

FIG. 13. The γ-ray detection efficiency from $K_{\pi 2}$ events. The points show the absolute detection efficiency determined from the conversion length method. The solid histogram is the γ-ray energy spectrum from events with one or two γ rays normalized, for the purpose of comparison, in the last five bins.

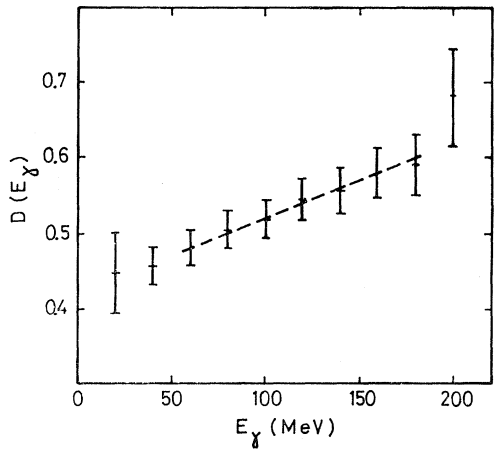

FIG. 14. The absolute γ-ray detection probability from $K_{\mu 3}$ events using the conversion-length method.

the allowed energy range for each value of the π^0 energy. This leads to the curve given in Fig. 15, which shows the absolute π^0 detection efficiency as a function of energy. The quick fall observed between 145 and 155 MeV is due to the 50-MeV cut on the energy of the γ rays. Since the determination of ξ is very sensitive to the shape of the π^0 spectrum for the lower values of the π^0 energy, all events with E_π smaller than 155 MeV have been removed from the analyzed sample. In the accepted zone of the Dalitz plot, the relative variation of the π^0 detection efficiency never exceeds 10%.

The final sample, after all cuts, consists of 3240 events.

3. Form-Factor Analysis

The analysis has been carried out using maximum-likelihood methods. Several kinds of distributions have been studied, for which the meaning of (s), the area over which the normalization is taken, is different. In forming the likelihood function $\mathcal{L}$, the muon detection efficiency is left out of the expression (3) since the events have been selected so that $\epsilon(E_\mu)$ is unity. The likelihood function is defined from

$$\mathcal{L}(\xi,\lambda_+;\beta)=\exp\left[-\frac{(\beta-\beta_0)^2}{2\sigma_\beta^2}\right] \times \prod_{\text{all events}} \frac{\rho(E_\pi{}^i,E_\mu{}^i;\xi,\lambda_+)D(E_{\gamma 1}{}^i,\beta)D(E_{\gamma 2}{}^i,\beta)}{\int\int_{(s)}\rho(E_\pi,E_\mu;\xi,\lambda_+)\epsilon'(E_\pi,\beta)dE_\pi dE_\mu}. \quad (5)$$

The exponential factor is included to allow for the uncertainty in the parameter β describing the relative γ-ray detection efficiency, β_0 and σ_β being its most likely value (2.3 GeV^{-1}) and the error (0.6 GeV^{-1}), respectively. The optimum values of the form factors are found by maximizing the function $\mathcal{L}(\xi,\lambda_+)$, which is itself obtained by maximizing $\mathcal{L}(\xi,\lambda_+;\beta)$ with respect to β at each value of (ξ,λ_+), i.e.,

$$\mathcal{L}(\xi,\lambda_+)=\mathcal{L}(\xi,\lambda_+;\beta'), \text{ where } \left.\frac{\partial\mathcal{L}(\xi,\lambda_+;\beta)}{\partial\beta}\right|_{\beta=\beta'}=0. \quad (6)$$

In practice it is more convenient to work with the logarithm of $\mathcal{L}$.

a. Muon spectra at fixed π^0 energies. A first step in the determination of the form factors is the analysis of the muon energy spectra at fixed π^0 energies; this has the advantage of being independent of the π^0 detection efficiency and avoids the problem of the double solution. A maximum likelihood analysis has been performed on the sample of 4347 events remaining after the application of all the above cuts apart from the one on the γ-ray energy which is not necessary since the events have been selected so that the muon and pion detection efficiencies are uncorrelated. Also, since only the muon spectra are studied, then terms in the likelihood function due to the π^0 detection efficiency can be dropped and

$$\ln\mathcal{L}_\mu=\sum_{\text{all events}}\ln\left[\frac{\rho(E_\pi{}^i,E_\mu{}^i;\xi,\lambda_+)}{\int\rho(E_\pi{}^i,E_\mu;\xi,\lambda_+)dE_\mu}\right],$$

where the normalization integral is taken from 155 to 197 MeV.

From the Dalitz-plot density expression it follows that the likelihood function $\mathcal{L}_\mu$ at fixed pion energies is independent of the factor $f_+(q^2)$ and hence of λ_+. The likelihood plot of the two remaining parameters Λ and $\xi(0)$ is shown in Fig. 16. As expected, no parasitic solution appears on this plot. The sensitivity to the q^2 variation of ξ is low; if ξ is assumed to be constant ($\Lambda=0$), the result is

$$\xi=-0.6_{-0.4}{}^{+1.2}.$$

b. Total density analysis in intervals of q^2. The second step is a total density analysis, dividing the Dalitz plot into q^2 bins and supposing ξ to be constant in each band. The advantages are the quasi-independence of the results on the π^0 detection efficiency. It is essentially an attempt to check the hypothesis of the linear q^2 dependence of ξ. In each band $(\Delta E_\pi)_j$, the likelihood function $\mathcal{L}_j$ defined by Eqs. (5) and (6) was computed. Taking bins of constant width $\Delta q^2=m_\pi{}^2$, the result, which is almost independent of λ_+, is shown in Fig. 17

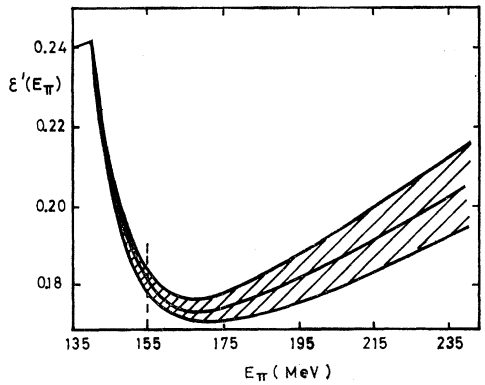

FIG. 15. The π^0 detection efficiency in $K_{\mu 3}$ events. The curves limiting the hatched region represent the detection efficiencies computed from the extreme variations of the γ-ray detection probability allowed within 1 standard deviation.

for λ_+ equal to 0.029. It is clear that with our statistics it is impossible to check accurately the hypothesis of linearity. The best fit for a straight line has a probability of 32%.

c. Total density analysis. The preceding methods use only part of the available information. As a third step, the variation of density with the energy of both the pion and the muon through the entire selected part of the Dalitz plot has been studied. The analysis was performed with the 3240 events remaining after cuts.

The likelihood function defined by Eqs. (5) and (6) has been computed; the normalization integral is made over the accepted energy ranges ($155<E_\mu<197$ MeV, $155<E_\pi<235$ MeV).

As foreseen, when searching for the set of three parameters maximizing the likelihood function, one finds two solutions. The most likely values are

$$\lambda_+=0.055\pm0.025,\quad \xi(0)=-0.5\pm1.6,\quad \Lambda=-0.04\pm0.24.$$

These values fit the Dalitz-plot density observed with a χ^2 of 36.8 for 28 degrees of freedom. The quoted errors give the uncertainty on each parameter computed from its marginal distribution, i.e., evaluated independently of the others. They are obtained by subtracting 0.5 from the logarithm of the maximum value of the likelihood function, and include the small contribution of the uncertainty on the π^0 detection efficiency.

The result of the three-parameter fit is shown in Fig. 18(a). The 1-standard-deviation surface resembles a very thin oblique ellipsoid, showing that the parameters $\xi(0)$ and Λ are strongly correlated.

Figure 19 shows contours of the same logarithmic likelihood function on a scale large enough to include the parasitic solution. For $\lambda_+=0.055$ this solution

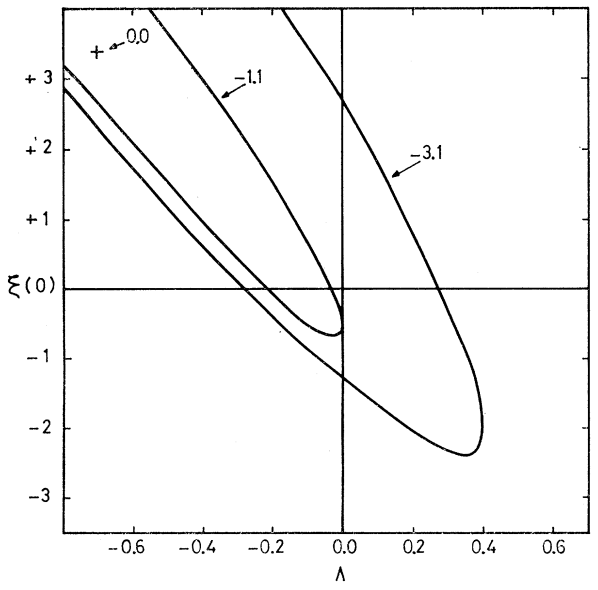

FIG. 16. Muon energy spectra analysis at fixed π^0 energies. The curves show the 1- and 2-standard-deviation contours of the two-parameter logarithmic likelihood function.

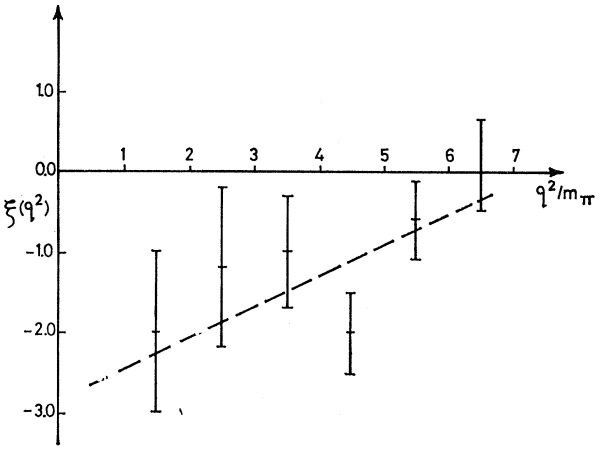

FIG. 17. Total density analysis in bins of q^2. The best linear fit is shown and has a χ^2 of 4.7.

appears as a ridge displaced by $\Delta\xi(0)\simeq-3.0$ with respect to the "principal solution" shown in Fig. 18(a). The most likely values of this second solution are $\xi(0)=-1.5$ and $\Lambda=-0.35$, but at that point the likelihood function $\ln\mathfrak{L}$ is lower by 8.6 with respect to the first solution, the corresponding ratio of probabilities being 2×10^{-4}. If larger values of λ_+ are allowed, the difference decreases but the absolute value of Λ becomes very high; for $\lambda_+\sim0.1$ both solutions reach approximately the same probability, but the parasitic solution is at $\Lambda=-0.8$. So far, these values can be considered as unreasonable. Furthermore, any solution of this type is ruled out by the results of the analysis of the muon energy spectra at fixed pion energies described above. Further discussion is therefore limited to the more likely solution.

For each λ_+ value, $\xi(0)$ and Λ can be replaced by uncorrelated parameters (see Appendix C) that can be taken as $\xi(0)$ and $\xi(6.8m_\pi^2)$ as illustrated in Fig. 18(b). The most likely values are

$$\lambda_+=0.055\pm0.025,\quad \xi(0)=-0.5\pm1.5,$$
$$\xi(6.8m_\pi^2)=-0.08\pm0.50.$$

The variation of the result for $\xi(6.8m_\pi^2)$ with λ_+ can be well approximated by the linear expression

$$\xi(6.8m_\pi^2)=-19\lambda_++0.20$$

if the range of λ_+ is limited to between 0.02 and 0.05.

This expression emphasizes the strong λ_+ dependence of our ξ determination. If λ_+ is fixed at 0.029, the value obtained from a compilation of previous K^+ experimental data,[8] one gets[13]

$$\lambda_+=0.029,\quad \xi(0)=0.2\pm2.0,\quad \xi(6.8m_\pi^2)=-0.35\pm0.21.$$

The corresponding χ^2 is 38.6 for 29 degrees of freedom (an increase of 1.8 compared to the optimum three-parameter fit with one more degree of freedom).

[13] Since λ_+ is fixed, only two parameters are fitted, and the error in $\xi(6.8m_\pi^2)$, which is strongly correlated with λ_+, becomes much smaller.

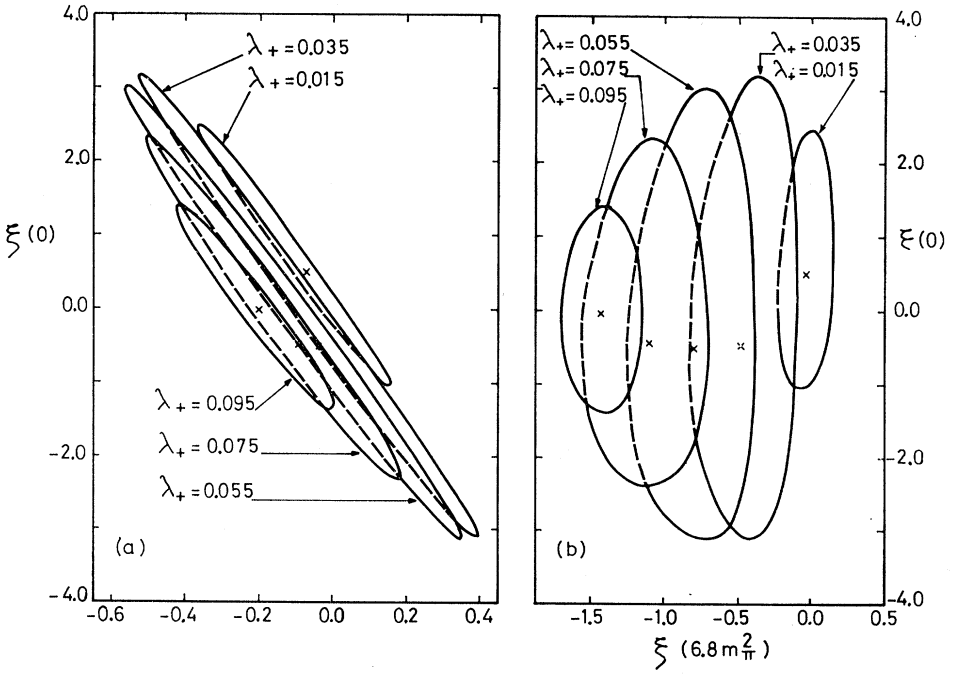

FIG. 18. Three-parameter analysis of the Dalitz-plot density in terms of (a) λ_+, $\xi(0)$, and Λ; (b) λ_+, $\xi(0)$, and $\xi(6.8m_\pi^2)$. The contours are drawn for several values of λ_+ and give the limits of the volume inside which there is a 68% probability of finding the three parameters simultaneously. This volume is defined by $(\ln\mathcal{L}_{\max}-\ln\mathcal{L})<1.8$.

Finally, fixing $\lambda_-=0$, the two-parameter likelihood function for $\xi(0)$ and λ_+ is shown in Fig. 20. The variables are correlated; the most likely values are

$$\xi(0)=-1.1\pm0.5, \quad \lambda_+=0.050\pm0.018.$$

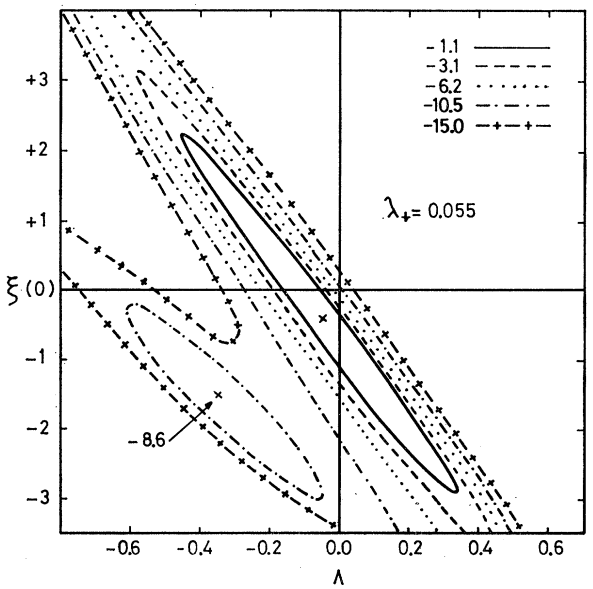

FIG. 19. Two-parameter plot in terms of $\xi(0)$ and Λ, of the logarithmic likelihood function for the complete Dalitz-plot density analysis, assuming $\lambda_+=0.055$ and showing the parasitic solution. Equal-likelihood contours are drawn, $\ln\mathcal{L}$ having been normalized to zero at its maximum value. The five contours shown would correspond, if $\xi(0)$ and Λ were normally distributed, to the 1-, 2-, 3-, 4-, and 5-standard-deviation levels.

C. Muon Polarization

In $K_{\mu3}$ decay, the polarization $\mathcal{P}$ of the muon is total. The expression for $\mathcal{P}$, given in Appendix B, is a function of the kinematical variables (E_π,E_μ) and of the ratio $\xi(q^2)=f_-(q^2)/f_+(q^2)$ only. Hence $\xi(q^2)$ can be estimated from the polarization measurement without any assumptions for the q^2 dependence of $f_\pm(q^2)$. In the following analysis, the results for the two parameters $\xi(0)$ and Λ need no knowledge of λ_+ or λ_-. However, the parameters are related by $\Lambda=\xi(0)(\lambda_--\lambda_+)$; thus a constraint on one of them (for example $\lambda_-=0$) can lead to a determination of the other (λ_+).

A measurement of the component of the muon polarization perpendicular to the decay plane, odd under T and proportional to $\mathrm{Im}\xi$, allows a direct test of the validity of time reversal invariance in weak interactions.

In this experiment, a sample of fully reconstructed $K_{\mu3}$ events, with two converted γ rays and a stopping muon, is available. The positron produced in the μ^+ decay can be used as a polarization analyzer, and the μ polarization at each point of the Dalitz plot can be studied. This study obviously requires no knowledge of the Dalitz-plot density, and hence the estimation of ξ by this method does not depend on the muon or pion detection efficiencies.

1. Method of Analysis

In the absence of a magnetic field, the distribution in momentum and emission angle of the positron with

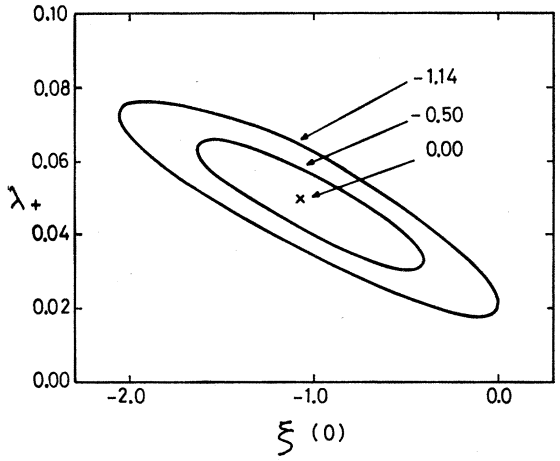

FIG. 20. Two-parameter plot in terms of $\xi(0)$ and λ_+ of the logarithmic likelihood function for the complete Dalitz-plot density analysis, assuming $\lambda_-\equiv 0$.

respect to the polarization vector $\mathcal{P}$ is given by

$$\frac{d^2N}{dxd(\hat{e}\cdot\mathcal{P})}=x^2(3-2x)[1-\alpha(x)(\hat{e}\cdot\mathcal{P})], \qquad (7)$$

where x is the ratio of the positron momentum to its maximum possible value and where

$$\alpha(x)=(1-2x)/(3-2x)$$

is the asymmetry coefficient.

From distribution (7), we can construct the likelihood function

$$\ln\mathcal{L}=\sum_{\text{all events}}\ln\{1-\alpha(x_i)[\hat{e}_i\cdot\mathcal{P}(E_\pi{}^i,E_\mu{}^i;\xi)]\}, \qquad (8)$$

where, as described in Appendix A,

$$\mathcal{P}=\mathcal{P}_L\hat{u}+\mathcal{P}_T\hat{t}+\mathcal{P}_N\hat{n}.$$

The likelihood function can be maximized either with respect to the polarization components $\mathcal{P}_L$, $\mathcal{P}_T$, and $\mathcal{P}_N$ or, alternatively, as a function of ξ.

In the presence of a magnetic field, directed along $\hat{B}$, only the polarization component parallel to the magnetic field is conserved and expression (8) becomes

$$\ln\mathcal{L}=\sum_{\text{all events}}\ln\{1-\alpha(x_i)(\hat{e}_i\cdot\hat{B})[\mathcal{P}(E_\pi{}^i,E_\mu{}^i;\xi)\cdot\hat{B}]\}. \qquad (9)$$

For a magnetic field as high as 1.9 T, depolarization of the muon due to ionization or to muonium formation can be neglected.[14]

Figure 21 illustrates the variation of the polarization vector as a function of (E_π,E_μ) and of ξ, which is taken to be independent of q^2. The expected precision of the measurements are also represented and it is seen that

[14] A. Buhler, T. Massam, Th. Muller, M. Schneegans, and A. Zichichi, Nuovo Cimento **39**, 812 (1965); **39**, 823 (1965).

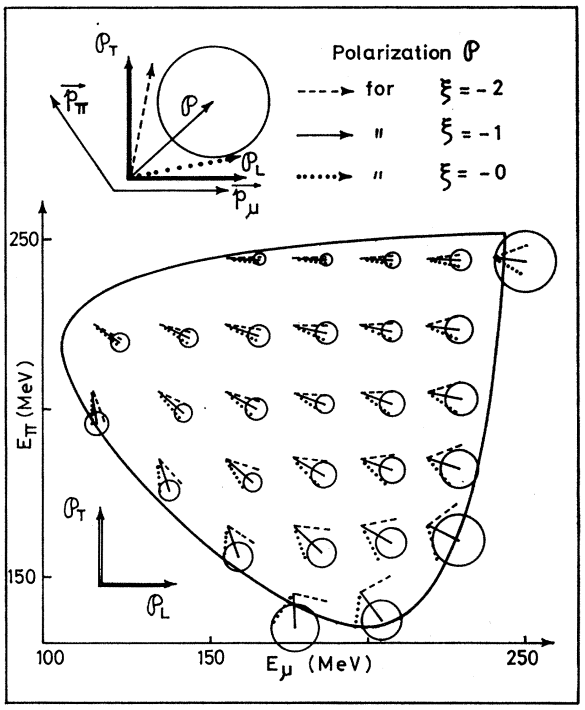

FIG. 21. Variation over the Dalitz plot of the polarization vector for three values of ξ. The circles represent, in each region, the expected errors in the determination of ξ (1 standard deviation), assuming a central value of $\xi=-1$ and taking a sample of events comparable in size to this experiment.

the events with small pion energy carry a high weight in the analysis.

2. Determination of Effective Asymmetry Parameter α

In the likelihood expression the effective asymmetry coefficient $\alpha(x_i)$ should be calculated for each event with the measured positron momentum, but in practice it has been replaced by its mean value because of the large measurement errors on the momentum of the positron. The theoretical mean value is $\bar{\alpha}_T=-0.33$, but as some low-energy electrons are lost or unmeasurable, the effective $\bar{\alpha}$ is expected to be different. In order to estimate this last value we have used samples of $K_{\mu 2}$ and $K_{\mu 3}$ events.

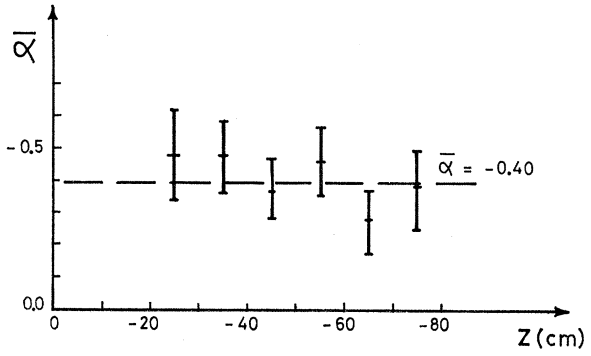

FIG. 22. Variation of the asymmetry parameter $\bar{\alpha}$ with the depth of the muon stopping point.

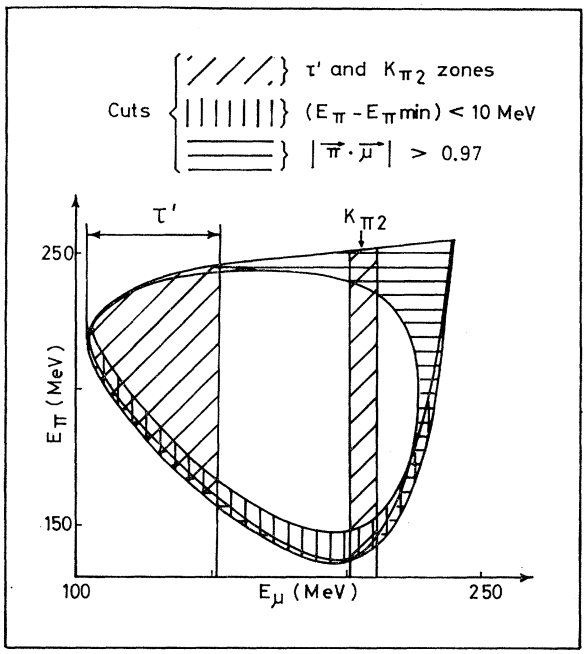

FIG. 23. Kinematical cuts applied for the polarization analysis.

Firstly, for a sample of 6000 $K_{\mu 2}^+$ events ($\mathcal{P}_L = -1$) we find $\bar{\alpha} = -0.36 \pm 0.03$. Secondly, if $\bar{\alpha}$ as well as ξ is left as a free parameter in the likelihood function, it is found that $\bar{\alpha}$ and ξ are uncorrelated and that the optimum value is

$$\bar{\alpha} = -0.40 \pm 0.04.$$

For the final calculation the asymmetry parameter $\alpha(x)$ in expression (9) has been replaced by $\bar{\alpha} = -0.40$.

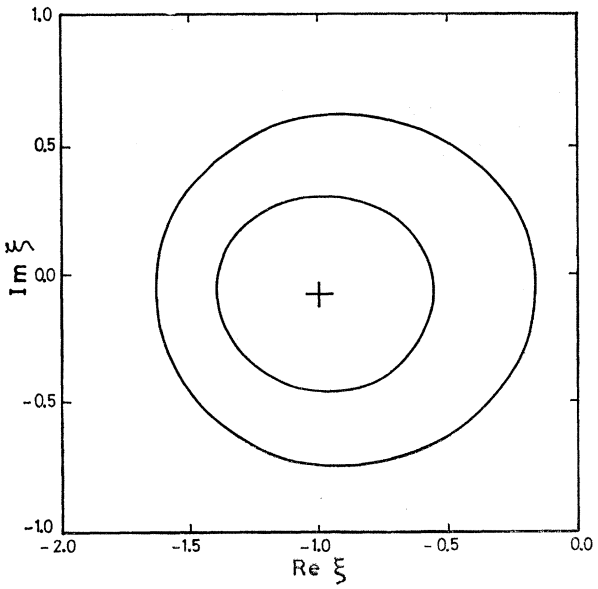

FIG. 24. Polarization analysis: 1- and 2-standard-deviation contours of the logarithmic likelihood function in Reξ and Imξ.

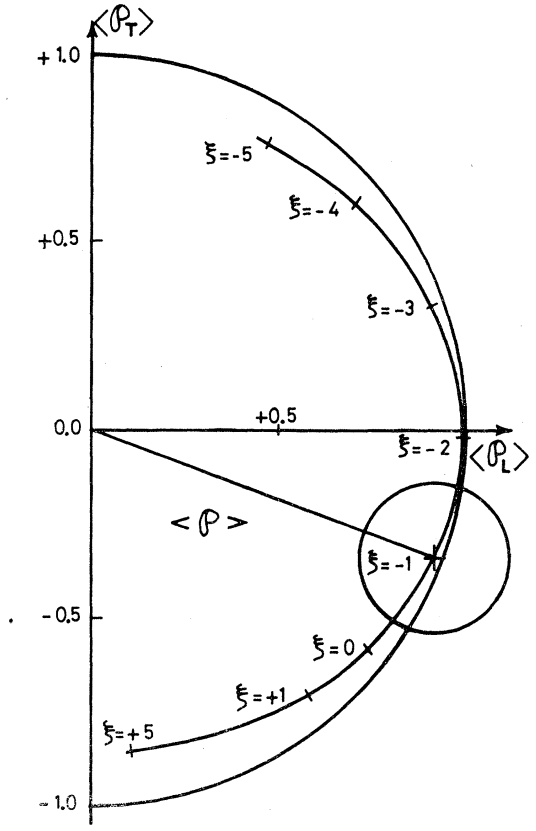

FIG. 25. Variation with ξ of the expected polarization, averaged over the regions of the Dalitz plot retained in this analysis. The circle represents the 1-standard-deviation contour in the likelihood function for $\langle \mathcal{P}_L \rangle$ and $\langle \mathcal{P}_T \rangle$.

3. *Sources of Systematic Bias*

From expression (9) it is clear that the two possible sources of bias are the following:

(i) An incorrect estimate of kinematical variables leading to an erroneous determination of $\mathcal{P}$ or a background due to another decay mode falsely classified as a $K_{\mu 3}$ event. As has been discussed above in Sec. III A, the general cuts imposed on the $K_{\mu 3}$ sample reduce such biases to very small effects.

(ii) A nonsymmetric detection efficiency in the variable $(\hat{e}\cdot\hat{B})$ which would modify the normalization of the probability density appearing in expression (9). This asymmetry can be due to an effective loss of decay positrons or to an incorrect measurement of $(\hat{e}\cdot\hat{B})$. Events with very steeply dipping tracks ($|\hat{\mu}\cdot\hat{B}| > 0.95$ or $|\hat{e}\cdot\hat{B}| > 0.95$) and events in which the muon stopped in the extreme regions of the chamber ($z_\mu < -80$ cm; $z_\mu > -10$ cm) have been removed from the sample. The electron angular distribution has been studied as a function of the muon stopping point and no asymmetry due to bad positron detection or measurement was observed. The parameter $\bar{\alpha}$ depends critically on the positron detection efficiency and this parameter was effec-

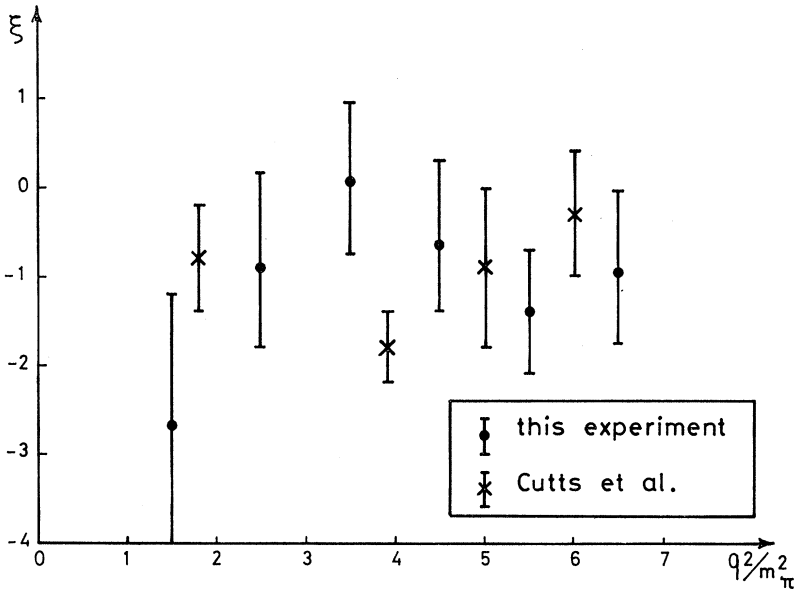

FIG. 26. Polarization analysis: the most probable value of ξ in each q^2 interval for this experiment and for the experiment of Cutts *et al.*, Ref. 16.

tively independent of the depth in the chamber at which the muon stopped, as is shown in Fig. 22.

Several cuts, supplementary to those already described in Sec. III A, were introduced for the muon polarization analysis.

a. Cut on angle $(\mathbf{p}_\pi,\mathbf{p}_\mu)$. If the angle ϕ between $\mathbf{p}_\pi$ and $\mathbf{p}_\mu$ is close to zero or 180°, the decay plane and hence the muon polarization vector are not well determined. In order to avoid such configurations, a cut $|\cos\phi|<0.97$ was introduced.

b. Lower border of Dalitz plot. From a study of Fig. 21, one can easily deduce that the polarization of the muon varies very rapidly with ξ and with (E_π,E_μ) near the lower border of the Dalitz plot; a small measurement error may thus introduce a large error in ξ in this zone. Taking our mean errors of measurements into account (see Sec. I), events falling in a zone of 10 MeV above the lower border of the Dalitz plot were rejected.

The three kinematical cuts, on the muon range the angle between the muon and pion, and the Dalitz-plot lower border are shown in Fig. 23.

After all cuts, we keep 5964 $K_{\mu 3}$ events, fully reconstructed and having a well-visible $\mu^+ \rightarrow e^+$ decay.

4. Results

The following results were obtained from a maximum likelihood analysis of polarization of the muons in the final sample of events.

a. Constant form factors.

(i) Normal polarization $\mathcal{P}_N$ and imaginary part of ξ. The form factor ratio ξ is a complex number if no time-reversal invariance is postulated. The result of an analysis in terms of $\mathrm{Re}\xi$ and $\mathrm{Im}\xi$ is shown in Fig. 24. The errors on these parameters, which are uncorrelated, are obtained from their marginal distributions. The result is

$$\mathrm{Re}\xi=-1.0\pm0.3,$$
$$\mathrm{Im}\xi=-0.1\pm0.3.$$

This value of $\mathrm{Im}\xi$ corresponds to a mean value of the polarization normal to the $K_{\mu 3}^+$ decay plane of

$$\bar{\mathcal{P}}_N=-0.03\pm0.09.$$

This result is consistent with T invariance, as was a previous, less accurate, experiment using the muon polarization in charged K decays.[15] Three such experiments for K_L^0 decay also reach this conclusion,[3] in one case with a better accuracy.

(ii) Polarization in the decay plane and the real part of ξ. Assuming that the interaction is invariant under time reversal, then the most likely value of ξ, assumed to be constant, is

$$\xi=-1.0\pm0.3.$$

The corresponding average values of the polarization components in the decay plane are

$$\bar{\mathcal{P}}_L=0.95\pm0.09,$$
$$\bar{\mathcal{P}}_T=-0.29\pm0.09.$$

These results are illustrated in Fig. 25 which shows, for our $K_{\mu 3}$ sample, the variation of the expected average polarization components as a function of ξ.

b. Study of q^2 dependence of ξ. In order to study the variation of ξ on the four-momentum transfer to the lepton system, we have subdivided our sample into

[15] A. C. Callahan, U. Camerini, R. D. Hantman, R. H. March, D. L. Murphree, G. Gidal, G. E. Kalmus, W. M. Powell, C. L. Sandler, R. T. Pu, S. Natali, and M. Villani, Phys. Rev. 150, 1153 (1966).

slices of q^2. The results are shown in Fig. 26 in which we have also drawn for comparison the results of another experiment[16] measuring the $K_{\mu 3}^+$ muon polarization. No strong deviation from linearity appears to exist and a first-order development of $\xi(q^2)$ [Eq. (1)] does not appear to be unjustified. Making a two-parameter likelihood analysis in terms of $\xi(0)$ and Λ, the result is

$$\xi(0)=-0.6\pm1.1, \quad \Lambda=-0.07\pm0.35.$$

Contours of the likelihood function are shown in Fig. 27(a); the correlation observed can be removed by parametrizing $\xi(q^2)$ in terms of $\xi(0)$ and $\xi(4.9m_\pi^2)$ as is seen in Fig. 27(b).

The results of a two-parameter fit to the muon polarization data are thus best expressed as

$$\xi(0)=-0.6\pm1.1, \quad \xi(4.9m_\pi^2)=-1.0\pm0.3,$$

or, alternatively, as

$$\xi(4.9m_\pi^2)=-1.0\pm0.3, \quad \Lambda=-0.07\pm0.35.$$

All of the results quoted above need no assumption as to the value of λ_+.

With the assumption $\lambda_-=0$, the polarization measurements have been analyzed in terms of $\xi(0)$ and λ_+. As can be seen from Fig. 28, the result is a linear relationship between the parameters.

IV. SCALAR AND TENSOR COUPLINGS

The preceding analysis has been performed in the frame of the $V-A$ theory. If no hypothesis is made about the nature of the currents, the more general matrix element has the form described in the Introduction, which is formally identical to the one obtained for pure vector interaction, but with f_+ and $\xi=f_-/f_+$ replaced as follows:

$$f_+ \rightarrow F_+=f_+ + \frac{m_l}{m_K} f_T$$

$$\xi \rightarrow \Xi=\left\{\xi+\frac{2m_K}{m_l}R_S\left[\frac{m_l}{m_K}+\frac{2(E_\nu-E_l)}{m_l}\right]R_T\right\}\Big/\left(1+\frac{m_l}{m_K}R_T\right),$$

where $R_S=f_S/f_+$ and $R_T=f_T/f_+$ may be q^2 dependent.

The number of parameters involved is such that, despite our large statistics, a complete analysis with all form factors and their q^2 dependence would be meaningless. A possible q^2 dependence of f_+ will be maintained ($\lambda_+\neq0$) but ξ, R_S, and R_T will be considered as constant, each form factor $f_S(q^2)$, $f_T(q^2)$, $f_-(q^2)$, and $f_+(q^2)$ thus being supposed to have the same q^2 dependence. The vector coupling will be considered to be always present with possible admixtures of scalar or tensor terms, but not all three types simultaneously.

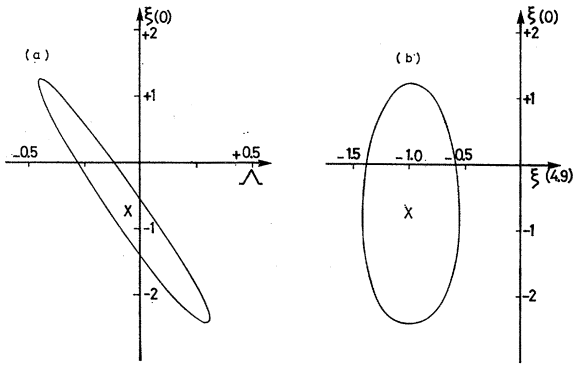

FIG. 27. Polarization analysis: two-parameter logarithmic likelihood functions showing the 1-standard-deviation contours for (a) the parameters $\xi(0)$ and Λ; (b) the uncorrelated parameters $\xi(0)$ and $\xi(4.9m_\pi^2)$.

A. Search for Scalar Contribution ($R_T=0$)

In the matrix element, ξ and R_S appear only in the linear combination $\xi+(2m_K/m_l)R_S$. Thus, when $K_{\mu 3}$ decay only is analyzed (μ^+ polarization or Dalitz-plot density) the measured quantities are λ_+ and

$$\xi+2\frac{m_K}{m_\mu}R_S=\xi+9.3R_S. \tag{10}$$

The branching ratio $\mathcal{R}$ involves $K_{\mu 3}$ and K_{e3} decay and it is given by

$$\mathcal{R}=\frac{S_\mu(\xi+9.3R_S,\lambda_+)}{S_e(R_S^2,\lambda_+)}. \tag{11}$$

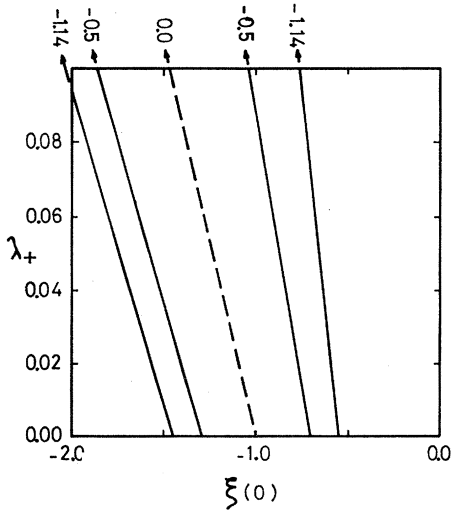

FIG. 28. Polarization analysis: two-parameter logarithmic likelihood function for $\xi(0)$ and λ_+, assuming $\lambda_-=0$. The dashed line represents the almost flat ridge which is the maximum.

[16] D. Cutts, R. Stiening, C. Wiegand, and M. Deutsch, Phys. Rev. Letters 20, 955 (1968).

Only R_S^2, and not ξ, enters into the K_{e3} term in the denominator, and the branching ratio gives a relationship between ξ and R_S which is different from the linear relation (10) from the $K_{\mu 3}$ analysis. An addition of the analyses therefore leads to a determination of R_S^2 or $|R_S|$ and, in general, to two values of ξ owing to the uncertainty in the sign of R_S. Figure 29 shows, for various hypotheses concerning λ_+, the 1-standard-deviation zones in the (R_S, $\xi+9.3R_S$) plot obtained from an addition of the $K_{\mu 3}$ polarization and Dalitz-plot likelihood functions and branching-ratio measurement. The determination of R_S is not very accurate, due to the fact that the two zones are nearly parallel; S_e being a function of R_S^2 then dS_e/dR_S vanishes at $R_S=0$ and, in both equations (10) and (11), it can be shown that

$$\left(\frac{d\xi}{dR_S}\right)_{R_S=0} = -9.3.$$

The results are as follows:

(1) For λ_+ fixed at 0.029, then, as illustrated in Fig. 29(a),

$$|R_S| = 0.08 \pm 0.07.$$

(2) If λ_+ is also allowed to vary, then the best fit, shown in Fig. 29(b), is obtained for

$$R_S = 0.00 \pm 0.15, \quad \xi = -1.0 \pm 1.5, \quad \lambda_+ = 0.060 \pm 0.020.$$

R_S being zero, only one value for ξ is obtained. As usual the errors quoted have been obtained from the marginal distribution of each variable and so, for this experiment, the upper limit on R_S is 0.15 at the 68% confidence level.

B. Search for Tensor Contribution ($R_S=0$)

It will be seen that most of the information about the presence of a tensor term R_T is provided by the Dalitz-plot distribution.

The sample of 3240 events used for the Dalitz-plot study has been analyzed by a maximum likelihood method with three parameters ξ, R_T, and λ_+.

The most likely set of values is

$$\lambda_+ = 0.05 \pm 0.02, \quad R_T = 0.05 \pm 0.25, \quad \xi = -0.75 \pm 0.5.$$

The $K_{\mu 3}$ polarization and the branching-ratio measurements individually add very little information on R_T. Essentially they each provide an approximately linear relationship between the permitted values of ξ and R_T,which may be expressed, respectively, as

$$\xi + 2.5R_T = (-1.0 \pm 0.3)$$

and

$$\xi + 2.1R_T = (-0.40 \pm 0.20) - 10\lambda_+.$$

However, the result on R_T obtained from the Dalitz-plot analysis can be improved by taking into account the restrictive relationships provided by the polarization and branching-ratio analyses. The three likelihood functions have been added. The result found for R_T is strongly λ_+ dependent, as illustrated in Fig. 30. The best fit is obtained for

$$\lambda_+ = 0.060 \pm 0.025, \quad R_T = 0.00 \pm 0.22, \quad \xi = -1.00 \pm 0.65.$$

The upper limit within 68% confidence for R_T is 0.22.

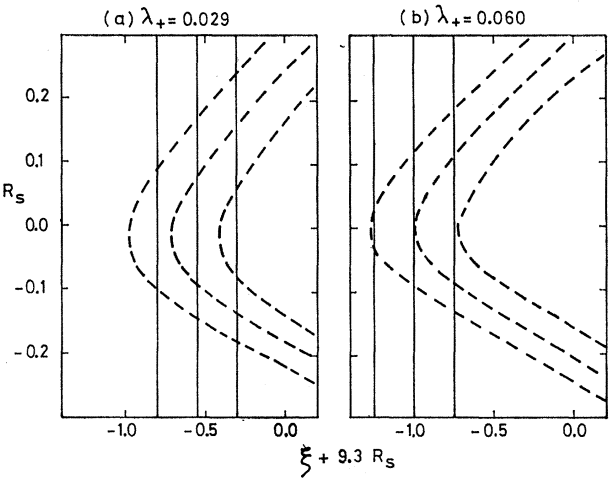

FIG. 29. The 1-standard-deviation bands are shown for the branching ratio (dashed line) and for the combined Dalitz-plot and polarization data (full lines) assuming that (a) $\lambda_+=0.029$ and (b) $\lambda_+=0.060$, its optimum value.

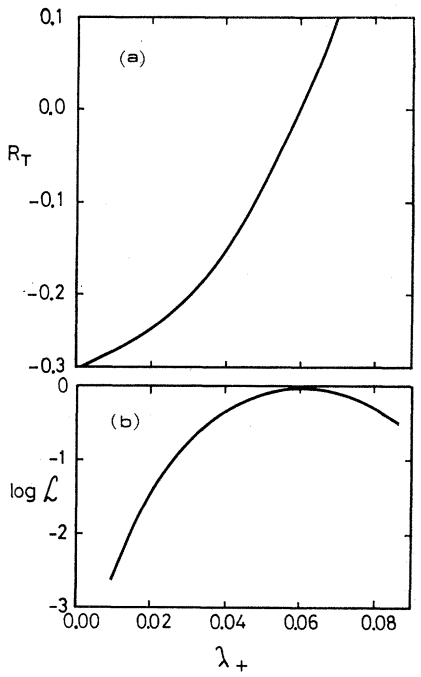

FIG. 30. (a) Most likely value of R_T as a function of λ_+, and (b) corresponding values of the natural logarithm of the likelihood function.

TABLE III. Values of ξ measured in this experiment for $\lambda_+ \equiv 0.029$.

Method of analysis	One-parameter fit ξ	One-parameter fit $d\xi/d\lambda_+$	Two-parameter fit Uncorrelated parameters	Two-parameter fit $d\xi/d\lambda_+$
Muon polarization in $K_{\mu 3}^+$	-1.0 ± 0.3	0	$\xi(0.0m_\pi^2) = -0.6 \pm 1.1$	0
			$\xi(4.9m_\pi^2) = -1.0 \pm 0.3$	0
$K_{\mu 3}^+/K_{e3}^+$ branching ratio	-0.72 ± 0.21	-10	$\xi(3.9m_\pi^2) = -0.72 \pm 0.21$	-10
$K_{\mu 3}^+$ Dalitz plot	-0.35 ± 0.21	-19	$\xi(0.0m_\pi^2) = -0.2 \pm 2.0$	-20
			$\xi(6.8m_\pi^2) = -0.35 \pm 0.21$	-19
Combined result	-0.65 ± 0.13	-11	$\xi(0.0m_\pi^2) = -1.2 \pm 0.5$	$+5$
			$\xi(5.1m_\pi^2) = -0.65 \pm 0.13$	-11

C. Conclusions

We find no evidence for the existence of scalar or tensor currents, confirming earlier experiments. The most accurate previous limits for either coupling have come from studies of K_{e3}^+ decay. For the scalar coupling, Bellotti *et al.*[17] obtained a limit $R_S < 0.18$ with 90% confidence, a little more accurate than that quoted here. For the tensor term our limit, derived almost entirely from the $K_{\mu 3}^+$ decay, is slightly more accurate than that of Botterill *et al.*,[18] who quote $R_T < 0.58$ with 90% confidence.

A more complete survey of earlier work on this topic has recently been presented by Rubbia.[8]

V. CONCLUSIONS

In this section the discussion is restricted to vector contributions to the matrix element, which is assumed to be T invariant. Other types of coupling were considered in Sec. IV and the polarization measurements reported here and elsewhere show no evidence for T violation. The results of the three methods of analysis are combined and compared with other experiments and with theoretical predictions.

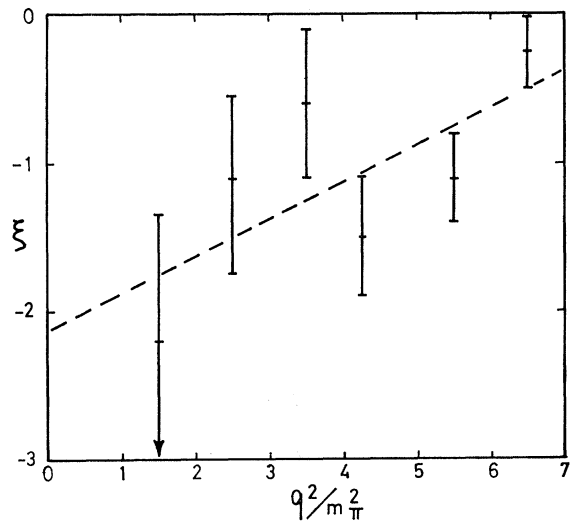

FIG. 31. Determination of ξ in q^2 bins obtained from the addition of polarization and Dalitz-plot data.

A. Combination of Results of this Experiment

It has been seen in the previous sections that each separate method could provide a rather accurate result for ξ at one point in the q^2 interval, but rather poor information about the slope of the q^2 dependence. Our aim in this combined analysis is to exploit all the information on the q^2 variation of form factors contained in our data. Nevertheless, the evaluation of the parameters describing the form factors will be complicated by the strong correlations which appear, especially between ξ and λ_+. Consequently the results are studied in four stages: with no assumption for the shape of $\xi(q^2)$; with λ_+ fixed; with λ_+ free to vary; and, finally, in the "f,f_+" parametrization ($\lambda_-=0$).

1. No Assumption for Shape of $\xi(q^2)$

Some information about the q^2 dependence of the form factor ratio $\xi(q^2)$ can be obtained without any assumption about the shape of this dependence. As explained in Secs. III B and III C, this can be accomplished by dividing the Dalitz plot in π^0 energy (or q^2) bands and searching for a constant ξ in each band. The polarization result is independent of λ_+, and the Dalitz-plot data, analyzed in this manner, is quasi-independent; the addition of these data is shown in Fig. 31. The best fit under the assumption that ξ is constant is obtained for

$$\xi = -0.82 \pm 0.16$$

and has a χ^2 probability of 4%. If a linear q^2 dependence of ξ is introduced, then the best fit, shown in the figure, has a probability of 18% and is parametrized by

$$\xi(5.2m_\pi^2) = -0.82 \pm 0.16, \quad \Lambda = 0.25 \pm 0.11.$$

This analysis is obviously not sufficient to prove the linearity of $\xi(q^2)$ but it permits it to be adopted as the simplest hypothesis.

[17] E. Bellotti, E. Fiorini, and A. Pullia, Nuovo Cimento 52A, 1287 (1967).

[18] D. R. Botterill, R. M. Brown, A. B. Clegg, I. F. Corbett, G. Culligan, J. McL. Emmerson, R. C. Field, J. Garvey, P. B. Jones, N. Middlemas, D. Newton, T. W. Quirk, G. L. Salmon, P. Steinberg, and W. S. C. Williams, Phys. Rev. 174, 1661 (1968).

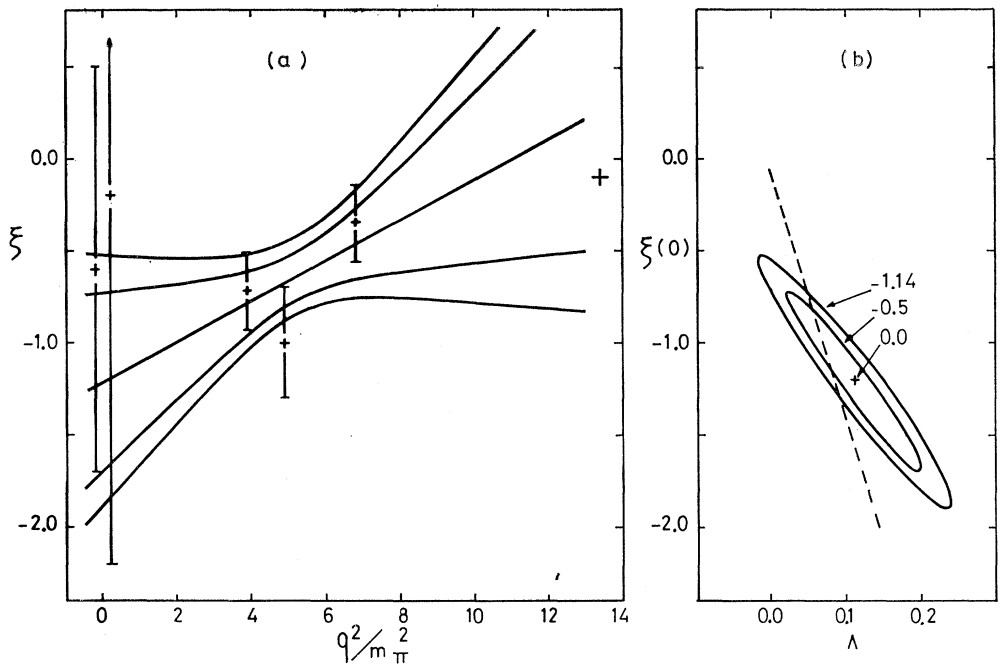

FIG. 32. Over-all fit of the results of the three methods, for $\lambda_+=0.029$. (a) ξ as a function of q^2, showing the five experimentally determined points and the best linear fit. The inner hyperbola provides the 1-standard-deviation error on ξ at each value of q^2 (one-parameter fit). The outer hyperbola is the envelope of all the linear fits to $\xi(q^2)$ which are within 1 standard deviation of the best fit (two-parameter fit). (b) Contours of the over-all likelihood function obtained by addition of the likelihood function for each method. The point at $q^2=13.4m_\pi^2$ in (a) and the dotted line in (b) represent the Callan-Treiman prediction; see text.

2. λ_+ *Fixed*

Table III summarizes the results for ξ described in the preceding sections, under the assumption that λ_+ is exactly equal to its world average value of 0.029. These are quoted in each case both for a constant ξ and for a ξ varying linearly with q^2. The values of $d\xi/d\lambda_+$, evaluated at $\lambda_+=0.029$, are also given and they show that any deviation of λ_+ from its presently accepted value could appreciably vary the results of the branching-ratio and Dalitz-plot experiments.

If ξ is assumed to be constant, the mean value is

$$\xi=-0.65\pm0.13 \quad \text{for} \quad \lambda_+\equiv0.029.$$

The χ^2 of the fit is 2.94 for two degrees of freedom. If ξ were constant, then the probability that the χ^2 exceeds 2.9 is 23%. Therefore, for $\lambda_+=0.029$, the hypothesis that ξ be constant is in reasonable agreement with our data.

If a q^2 dependence of ξ is looked for (two-parameter fit), then either addition of the three likelihood functions or the fit of a straight line to the data displayed in Table III lead to the results shown in Fig. 32. The best values for the parameters $\xi(0)$ and Λ are

$$\xi(0)=-1.2\pm0.5, \quad \Lambda=0.11\pm0.09 \quad \text{for} \quad \lambda_+\equiv0.029,$$

where the errors give the uncertainty on each parameter computed from its marginal distribution (see Appendix D). In terms of uncorrelated parameters, one gets

$$\xi(5.1m_\pi^2)=-0.65\pm0.13, \quad \Lambda=0.11\pm0.09 \quad \text{for} \quad \lambda_+\equiv0.029.$$

The χ^2 probability for this fit is 55%.

3. λ_+ *Free*

We can go further in the analysis by leaving free the parameter λ_+ in order to estimate its value. Such a three-parameter analysis was previously described in Sec. III B for the Dalitz-plot data alone. The addition of the three likelihood functions allows a more accurate determination; the branching-ratio measurement provides a direct constraint between the three parameters, and the polarization result, although itself independent of λ_+, influences the fit due to the correlations between

TABLE IV. Values of ξ measured in this experiment for $\lambda_+\equiv0.060$.

Method of analysis	Uncorrelated parameters
Muon polarization in $K_{\mu 3}^+$	$\xi(0.0m_\pi^2)=-0.6\ \pm1.1$
	$\xi(4.9m_\pi^2)=-1.0\ \pm0.3$
$K_{\mu 3}^+/K_{e3}^+$ branching ratio	$\xi(3.9m_\pi^2)=-1.03\pm0.21$
$K_{\mu 3}^+$ Dalitz plot	$\xi(0.0m_\pi^2)=-0.5\ \pm1.5$
	$\xi(6.8m_\pi^2)=-0.88\pm0.21$
Combined result	$\xi(0.0m_\pi^2)=-1.0\ \pm0.5$
	$\xi(5.1m_\pi^2)=-0.97\pm0.13$

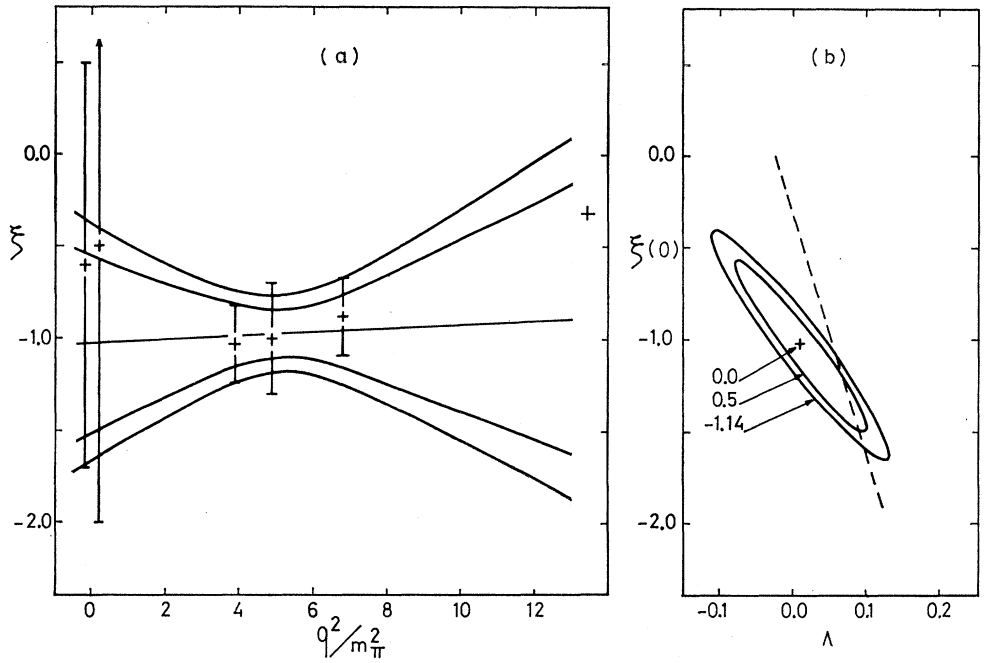

FIG. 33. Over-all fit of the results of the three methods, for $\lambda_+=0.060$. See the caption of Fig. 32.

λ_+, $\xi(0)$, and Λ. The best values of the three parameters are

$$\xi(0)=-1.0\pm0.5, \quad \Lambda=0.01\pm0.11, \quad \lambda_+=0.060\pm0.019.$$

In terms of uncorrelated parameters, the above result can be quoted as

$$\xi(5.1m_\pi^2)=-0.97\pm0.20, \quad \Lambda=0.01\pm0.11, \quad \lambda_+=0.060\pm0.019.$$

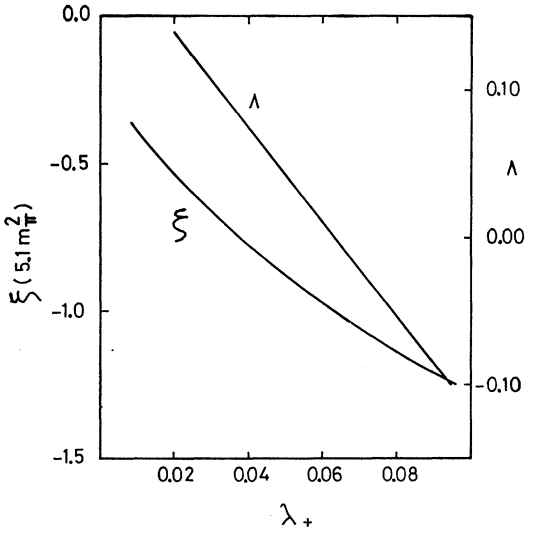

FIG. 34. Combined analysis: the dependence of $\xi(5.1m_\pi^2)$ and Λ on the value of λ_+.

For the optimum value $\lambda_+=0.060$, the results on ξ obtained from the three methods are displayed in Table IV and shown in Fig. 33. The errors on $\xi(0)$ and Λ in Fig. 33(b) are smaller than those quoted above, since they are computed assuming a fixed value $\lambda_+=0.060$. There is an excellent agreement between all three experiments.

However, it should be stressed that both $\xi(5.1m_\pi^2)$ and Λ are strongly correlated with λ_+. Figure 34 illustrates how the optimum values for these two parameters vary as λ_+ is changed.

4. $\lambda_-=0$

As was described in the Introduction, the model in which $f(q^2)$ and $f_+(q^2)$, the form factors corresponding to 0^+ and 1^- spin-parity amplitudes, are taken to have a linear q^2-dependence, is equivalent to setting $\lambda_-=0$. With this restriction, the addition of the likelihood functions from the three methods of analysis leads to the function shown in Fig. 35. The best estimation is

$$\xi(0)=-0.98\pm0.23, \quad \lambda_+=0.049\pm0.011 \quad \text{with} \quad \lambda_-\equiv0.$$

The parameter λ, describing the q^2 dependence of $f(q^2)$, is related to $\xi(0)$ and λ_+ by Eq. (2). Substituting, we obtain

$$\lambda=-0.030\pm0.012, \quad \lambda_+=0.049\pm0.011.$$

These two parameters are almost uncorrelated.

Summarizing the results presented above, and in particular Secs. V A 2 and V A 3, we can conclude that the values of ξ obtained in this experiment by the three methods of analysis (branching ratio, Dalitz plot,

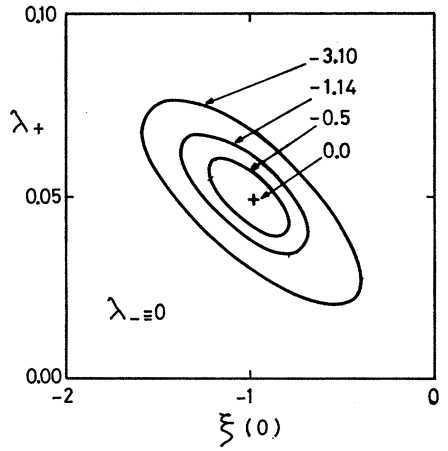

FIG. 35. Combined analysis: plot of the logarithmic likelihood function for $\xi(0)$ and λ_+ when $\lambda_-\equiv 0$, obtained from the addition of the functions shown in Figs. 8, 20, and 28.

and polarization) are completely compatible. Reasonable agreement between all the data is obtained with a value of λ_+ around 0.030 and with ξ constant. However, better fits are produced when

(a) λ_+ is held at this value and a linear q^2 variation of ξ is introduced;

(b) λ_+ is allowed to increase to about 0.060, even if ξ is constant.

B. Comparison with Previous Results

The results of form factor analyses in K decay have been frequently reviewed.[1,8,19] They have led to much discussion due to the fact that the value of ξ obtained from polarization measurements (about -1) was in disagreement with the quoted values determined from the branching ratios. The few Dalitz-plot density analyses were not accurate enough to bring significant additional information.

In this experiment, the self-consistency of all three methods appears in Sec. V A and the combined result agrees perfectly with all available polarization data. We thus disagree with most of the currently published values for the $K_{\mu 3}/K_{e3}$ branching ratio, and the Dalitz-plot analysis confirms that ξ is negative.

We will now compare our data to the most accurate results obtained separately with each method, from K^+ and K^0 decays, which must be described by the same form factors if the $\Delta I=\frac{1}{2}$ leptonic rule is valid. A more complete survey of earlier data may be obtained from the above-referenced review articles.

1. Polarization Measurements

The most recent and accurate experiments have been performed with counters or spark chambers,

[19] W. J. Willis, in *Proceedings of the Heidelberg International Conference on Elementary Particles, 1967*, edited by H. Filthuth (Interscience, New York, 1967), p. 273.

TABLE V. Determinations of ξ from μ^+ polarization.

Decay	Authors	ξ[a]
K^+	Cutts *et al.*, Ref. 16	-0.95 ± 0.30
	This experiment	-1.00 ± 0.30
K_L^0	Auerbach *et al.*[b]	$-1.2\ \pm0.5$
	Abrams *et al.*[c]	$-1.6\ \pm0.5$
	Helland *et al.*[d]	$-1.75_{-0.2}{}^{+0.5}$

[a] Results with an error of less than or equal to 0.5 are quoted.
[b] L. B. Auerbach *et al.*, Phys. Rev. Letters **17**, 980 (1966).
[c] R. J. Abrams *et al.*, Phys. Rev. **176**, 1603 (1968).
[d] J. A. Helland *et al.*, Phys. Rev. Letters **21**, 256 (1968).

using K^+ and K^0 decays. The results summarized in Table V have been obtained with hypothesis that ξ is constant. The agreement between the two K^+ measurements is excellent. The K_L^0 results tend to be lower but the difference is not statistically significant.

2. Branching-Ratio Determinations

The more accurate of the previous measurements of the branching ratios are summarized in Tables VI and VII for K^+ and K_L^0 decays, respectively.

Examination of the K^+ data shows that the ratio of the leptonic rates measured in this experiment is the lowest ever reported and, with its small error, is several standard deviations below the previous averaged value. This drop may be better understood when the separate leptonic decay fractions are compared.

The various reported ratios for the electronic mode K_{e3}^+ are in excellent agreement; only one experiment of the ten differs by more than 1 standard deviation from the mean value, and our result reproduces the previous average almost exactly. The K_{e3}^+ mode is the only important K^+ decay mode with a positron in the final state and it is relatively free from background.

TABLE VI. K^+ three-body leptonic branching ratios.

Authors	$K_{\mu 3}^+/K_{e3}^+$	$K_{\mu 3}^+/K_{\text{total}}^+$[a]	$K_{e3}^+/K_{\text{total}}^+$[a]
Taylor *et al.*[b]		$2.8\ \pm0.4$	
Roe *et al.*[c]			$5.0\ \pm0.5$
Shaklee *et al.*[d]	$0.63\ \pm0.10$	$3.0\ \pm0.5$	$4.7\ \pm0.3$
Borreani *et al.*[e]			$5.0\ \pm0.35$
Bisi *et al.*[f]		3.50 ± 0.15	
Callahan *et al.*[g]	0.703 ± 0.056	2.82 ± 0.19	4.02 ± 0.21
Auerbach *et al.*[h]	0.753 ± 0.076	3.82 ± 0.32	4.97 ± 0.16
Bellotti *et al.*[i]			$5.2\ \pm0.5$
Garland *et al.*[j]	$0.80\ \pm0.10$	$3.5\ \pm0.25$	$4.4\ \pm0.4$
Botterill *et al.*[k]	0.667 ± 0.017	3.28 ± 0.11	4.92 ± 0.21
Zeller *et al.*[l]	$0.81\ \pm0.13$	$3.5\ \pm0.6$	$4.4\ \pm0.4$
This experiment	0.596 ± 0.025	2.80 ± 0.11	4.75 ± 0.11

[a] Determinations with an error greater than 0.6 are omitted; some of these ratios have been computed from a quoted value of K_{l3}^+/K_τ^+ or $K_{l3}^+/K_{\mu 2}^+$ using $K_\tau^+/K_{\text{total}}^+=(5.57\pm0.04)\%$ and $K_{\mu 2}^+/K_{\text{total}}^+=(63.65\pm0.3)\%$.
[b] S. Taylor *et al.*, Phys. Rev. **114**, 359 (1959).
[c] B. P. Roe *et al.*, Phys. Rev. Letters **7**, 346 (1961).
[d] F. S. Shaklee *et al.*, Phys. Rev. **136**, B1423 (1964).
[e] G. Borreani *et al.*, Phys. Letters **12**, 123 (1964).
[f] V. Bisi *et al.*, Phys. Rev. **139**, B1068 (1965).
[g] A. C. Callahan *et al.*, Phys. Rev. **150**, 1153 (1966).
[h] L. B. Auerbach *et al.*, Phys. Rev. **155**, 1505 (1967).
[i] E. Bellotti *et al.*, Nuovo Cimento **52A**, 1287 (1967).
[j] R. Garland *et al.*, Phys. Rev. **167**, 1225 (1968).
[k] D. R. Botterill *et al.*, Phys. Rev. Letters **21**, 766 (1968).
[l] M. E. Zeller *et al.*, Phys. Rev. **182**, 1420 (1969).

TABLE VII. K_L^0 leptonic branching ratios.[a]

Authors	$K_{\mu 3}^0/K_{e3}^0$
Hopkins *et al.*[b]	0.81 ±0.08
Basile *et al.*[c]	0.62 ±0.05
Budagov *et al.*[d]	0.71 ±0.05
Evans *et al.*[e]	0.648±0.030
Beilliere *et al.*[f]	0.71 ±0.04

[a] Determinations with an error greater or equal than 0.10 are omitted.
[b] H. W. K. Hopkins *et al.*, Phys. Rev. Letters **19**, 185 (1967).
[c] P. Basile *et al.* (private communication).
[d] I. A. Budagov *et al.*, Nuovo Cimento **57A**, 182 (1968).
[e] G. R. Evans *et al.*, Phys. Rev. Letters **23**, 427 (1969).
[f] P. Beilliere *et al.*, Phys. Letters **30B**, 202 (1969).

Given this and the above experimental consistency, there can be little cause to doubt the result.

The ratios for the muonic mode $K_{\mu 3}^+$ show discrepancies considerably greater than their quoted errors. In trying to understand this spread in the measured values, it is important to remember that 90% of all K^+ decays involve a single charged particle which is either a muon or a pion, and that only about 1 in 30 of such decays is $K_{\mu 3}^+$; background problems are much more serious. In this experiment much attention was given to these difficulties. Only a small fraction of the film, that of best quality, was used; the scanning efficiency was very high and the consistency between the seven laboratories of the collaboration was completely satisfactory. The geometrical and kinematical cuts used and the size of the chamber ensured that all events in the analyzed momentum interval were recorded and that the background was reduced to 18%. Equally important, the background corrections could be accurately determined. Many of these could be computed in several ways and, even if overestimated by a factor of 2, would still leave a result significantly lower than the previous values.

3. Dalitz-Plot Density

Very few statistically important experiments have been carried out using this method: The π^0 spectra at fixed muon energies have been analyzed by Callahan *et al.*[15] with 444 $K_{\mu 3}^+$ decays observed in a heavy-liquid bubble chamber, and recently by Kijewski[20] using 2041 $K_{\mu 3}^+$ decays in spark chambers. Carpenter *et al.*[21] have given a result for the $K_{\mu 3}^0$ total Dalitz-plot density with 1371 events. The comparison between all these results is difficult because the definition of the fitted parameters and the hypotheses generally made to reduce their number vary with the authors. Furthermore, the strong correlation between ξ and λ_+ makes it necessary to choose a value of λ_+ when quoting a result on ξ, and this choice differs from one experiment to another. We compare in Table VIII the results derived from these publications for various one- and two-parameter fits. It must be stressed that some of the results in this table were not originally quoted by the authors concerned but have been derived by ourselves for the purpose of comparison. Such values are indicated by a footnote.

Comparing the various columns of the table, it is evident that the correlations between λ_+ and ξ are similar in the various experiments.

When a q^2 dependence of f_- is allowed ($\lambda_- \neq 0$), then it appears generally (Carpenter *et al.*, Kijewski, this experiment) that the result can be expressed as an accurate determination of ξ at a value of q^2 close to $7.0 m_\pi^2$, and a poor determination of $\xi(0)$. For $\lambda_+ = 0.029$, the combination of the three values gives

$$\xi(7.0 m_\pi^2) = -0.4 \pm 0.2 ,$$

with a χ^2 of 2.28 for two degrees of freedom. This leads to quite a good probability that the three experiments are internally consistent (33%). Comparison between other columns of Table VIII is not so good, but there is no evidence of a real disagreement.

4. General Discussion

It was shown above that the values of ξ determined in this experiment by the three methods of analysis are compatible. The polarization and Dalitz-plot measurements agree with previous work, and so this compatibility is clearly attributable to the low value determined for the branching ratio. We discuss briefly what the consequences will be if the previous high values of the branching ratio prove to be correct.

(a) Almost any set of ξ values can be explained if a sufficiently erratic variation of ξ with q^2 is postulated. However, such rapid variations are not experimentally proven (see, for example, Figs. 26 and 31 of this paper).

(b) If a linear q^2 dependence for ξ is assumed, then it has been shown that each method of analysis measures $\xi(q^2)$ effectively at a particular q^2 value (approximately 4, 5, and $7 m_\pi^2$ for branching-ratio, polarization, and Dalitz-plot measurements, respectively); these q^2 values should be similar for different experiments. The three results depend differently on λ_+, as is shown in Table III. A study of the measured values shows that, even for a high branching ratio, the fit is improved if values of λ_+ greater than 0.030 are considered. On the other hand, if λ_+ is about 0.030, no value of Λ (the q^2 dependence of ξ) will significantly improve the fit.

(c) If μ-e universality is not valid, then the apparent ξ value determined from the branching ratio will differ from those from the $K_{\mu 3}$ analyses, in a manner which depends on the breakdown.

(d) There may be small contributions from scalar or tensor currents. It was shown in Sec. IV that in this experiment the upper limit on either of these couplings is small. It is also significant that when both λ_+ and R_i ($i=S$ or T) were left free in the likelihood analyses, then in each case the optimum fit was found by increasing λ_+ and keeping $R_i \simeq 0$.

[20] P. K. Kijewski, Ph.D. thesis, LRL Report No. UCRL-18433, 1969 (unpublished).
[21] D. W. Carpenter, A. Abashian, R. J. Abrams, G. P. Fisher, B. M. K. Nefkens, and J. H. Smith, Phys. Rev. **142**, 871 (1966).

TABLE VIII. The results of Dalitz-plot analyses.

Authors	Decay	Number of events	One-parameter fits $\lambda_+=\lambda_-=0$	One-parameter fits $\lambda_-=0, \lambda_+=0.029$	Two-parameter fits λ_- free, $\lambda_+=0.029$	Two-parameter fits $\lambda_-=0, \lambda_+$ free
Carpenter *et al.*[a]	K_L^0	1371	$\xi=1.2\pm0.8$	$\xi(0)=0.6\pm0.8$[b]	$\xi(7m_\pi^2)=0.5\pm0.8$[b]	
Callahan *et al.*[c]	K^+	444	$\xi=0.7\pm0.4$	$\xi(0)=0.2\pm0.4$		$\lambda_+=0.00\pm0.035$ $\xi(0)=0.72\pm0.60$
Kijewski[d]	K^+	2041	$\xi=-0.3\pm0.3$	$\xi(0)=-1.0\pm0.3$	$\xi(7.1m_\pi^2)=-0.8\pm0.4$ $\xi(0)=-1.2_{-4.3}^{+3.4}$	$\lambda_+=0.009\pm0.025$ $\xi(0)=-0.5\pm0.8$
This experiment	K^+	3240	$\xi=0.4\pm0.2$	$\xi(0)=-0.5\pm0.2$	$\xi(6.8m_\pi^2)=-0.35\pm0.21$ $\xi(0)=0.2\pm2.0$	$\lambda_+=0.050\pm0.018$ $\xi(0)=-1.1\pm0.5$

[a] D. W. Carpenter *et al.*, Phys. Rev. 142, 871 (1966).
[b] The figure quoted has been calculated from the published results.
[c] A. C. Callahan *et al.*, Phys. Rev. 150, 1153 (1966).
[d] P. K. Kijewski, Ph.D. thesis, LRL Report No. UCRL-18433, 1969 (unpublished).

C. Comparison with Theory

Many theoretical calculations have been made to predict values of the form factors and their q^2 dependence; these involve dispersion relations, current algebra, and superconvergent sum rules. Some authors predict values of $f_\pm$ at unphysical points, while other theories depend on parameters whose values are not well known. We therefore limit this discussion to a few general remarks. Several comprehensive reviews exist,[22] and the intention has been to present the data in sufficient detail so that any required numbers can be extracted.

(1) Many theories in all classes make the assumption that the 0^+ and 1^- amplitudes are dominated by single poles corresponding to the hypothetical κ and the well-known $K^*(891)$. The latter requires

$$\lambda_+=(m_\pi/m_{K^*})^2=0.024,$$

a value rather close to previous measurements.

As quoted above, for this experiment

$$\lambda=-0.030\pm0.012,\quad \lambda_+=0.049\pm0.011.$$

A negative value for λ is incompatible with the dominance of the 0^+ amplitude by a single pole. Further, our high value of λ_+, considered with the recently reported experiment of Botterill *et al.*,[23] who find $\lambda_+=0.045\pm0.015$, suggests that in the 1^- amplitude also the agreement with the model is not so good as was previously claimed. In this context, Lo,[24] using an analogy with the nucleon electromagnetic form factors, has suggested that the form factors may have a "dipole" structure.

(2) Using current algebra, Callan and Treiman[25] derived the relationship

$$f_+ + f_- = F_K/F_\pi, \tag{12}$$

where F_K and F_π are the decay constants for the two-body leptonic decays of the K and π mesons, and where $f_\pm$ are evaluated at the unphysical point $m_\pi^2=0$, $q^2=m_K^2$. With the help of a smoothness assumption, such as partial conservation of axial-vector current (PCAC), one can argue that Eq. (12) should be good to within 10% at the real pion mass, but there still exists the problem of extrapolating beyond the physical q^2 region. If $f_+(q^2)$ is linear up to $q^2=m_K^2$, then Eq. (12) can be written[26]

$$\xi(m_K^2)=\frac{1.25}{1+\lambda_+ m_K^2/m_\pi^2}-1.$$

This point is shown on Figs. 32 and 33 for $\lambda_+=0.029$ and $\lambda_+=0.060$, respectively; in both cases, if ξ can be extrapolated then the prediction is satisfied.

In the physical region, as is apparent from the review paper of Weinberg,[22] all of the straightforward applications of current algebra predict values of ξ which are small in magnitude and slowly varying; this is in contradiction to the results of this experiment.

(3) Finally we note a calculation by d'Espagnat and Gaillard,[27] who extend the Fubini-Furlan sum rule[28] by assuming that the "$SU(3)$ leakage" matrix elements are negligible for finite q^2. They derive an expression for the 0^+ term, $f(q^2)$, which, in a linear approximation, leads to $\lambda=-0.019$, in agreement with the value measured in this experiment. However, as the authors appreciate, the correction to ξ due to leakage terms cannot be zero, but its magnitude and sign are difficult to estimate.

[22] S. Weinberg in Ref. 1, p. 253; C. Callan in Ref. 8, p. 263; M. K. Gaillard and L. M. Chounet, CERN Report No. 70-14, 1970 (unpublished).
[23] D. R. Botterill, R. M. Brown, A. B. Clegg, I. F. Corbett, G. Culligan, J. Mch. Emmerson, R. C. Field, J. Garvey, P. B. Jones, N. Middlemas, D. Newton, T. W. Quirk, G. L. Salmon, P. H. Steinberg, and W. S. C. Williams, Phys. Letters **31B**, 325 (1970).
[24] S. V. Lo, Nucl. Phys. **B7**, 68 (1968).
[25] C. G. Callan and S. B. Treiman, Phys. Rev. Letters **16**, 153 (1966).
[26] The value 1.25 is taken from B. Renner, in *Proceedings of the Lund International Conference on Elementary Particles, Lund, 1969*, edited by G. von Dardel (Berlingska, Lund, Sweden, 1969), p. 223.
[27] B. d'Espagnat and M. K. Gaillard, Phys. Letters **25B**, 346 (1967).
[28] S. Fubini and G. Furlan, Physics **1**, 229 (1965).

D. Cabibbo Angle

The measurement of the K_{e3}^+ absolute decay rate (Sec. II) provides an estimate of the Cabibbo angle relative to the vector transition for meson decays θ_V^M. The rate is given by[29]

$$\Gamma(K_{e3}^+)=\sin^2\theta_V^M(1+3.707\lambda_+)\times 7.42\times 10^7\ \text{sec}^{-1},$$

where $\sin\theta_V^M=f_+(0)\sin\theta$; here θ is the "bare" Cabibbo angle and $f_+(0)=1$ in the limit of exact $SU(3)$.

From the measured rate $\Gamma=(3.85\pm0.09)\times10^6$ sec^{-1} one obtains

$$\sin\theta_V^M=(0.229\pm0.003)(1+3.707\lambda_+)^{-1/2},$$

and so

$$\begin{aligned}\sin\theta_V^M&=0.218\pm0.004 \quad \text{for} \quad \lambda_+=0.029\pm0.010\\ &=0.206\pm0.006 \quad \text{for} \quad \lambda_+=0.060\pm0.019.\end{aligned}$$

The corresponding axial-vector angle is given by the two-body leptonic decay rates of the kaon and pion. One obtains[8] $\sin\theta_A^M=0.2655\pm0.006$, where θ_A^M is related to the "bare" Cabibbo angle by

$$\tan\theta_A^M=(F_K/F_\pi)\tan\theta.$$

Combining these results then, to a good approximation,

$$\begin{aligned}F_K/F_\pi f_+(0)&=1.23\pm0.02 \quad \text{for} \quad \lambda_+=0.029\pm0.010\\ &=1.30\pm0.03 \quad \text{for} \quad \lambda_+=0.060\pm0.019.\end{aligned}$$

This ratio is one in the limit of exact $SU(3)$.

ACKNOWLEDGMENTS

This review paper has combined the results of five years work of a large collaboration. The basis of this analysis has been the data obtained predominantly in the first few years of the experiment. Due to the length of the experiment, many physicists have contributed at various stages to specific topics. We wish to express our thanks to these people, without whose work this combined analysis would not have been possible: R. Aguilar-Lloret, M. Baldo-Ceolin, L. Behr, J. Bettels, F. Biffis, G. Borreani, A. Caforio, E. Calimani, S. Ciampolillo, D. C. Cundy, T. Eichten, A. Ferrer, K. Freundenreich, D. Gamba, C. Garelli, A. Haatuft, P. Heusse, G. A. T. de Jongh, L. Kluberg, P. Ladrón, G. London, R. Llosá, J. P. Lowys, F. Mattiolo, G. Miari, R. Møllerud, D. Morellet, G. Myatt, M. Nikolic, C. Pascaud, G. Rinaudo, H. Schepers, J. Schneps, K. Schultze, H. Steiner, and R. T. Van de Walle.

We are grateful to Professor M. Baldo-Ceolin, Professor H. Faissner, Professor C. Franzinetti, Professor L. Jauneau, Professor A. Lagarrigue, Professor L. Leprince-Ringuet, Professor M. Merlin, Professor L. Michel, Professor C. Ramm, Professor A. Rousset, and Professor B. Trumpy for their constant encouragement and interest in the experiment.

Finally, we thank the staff of the CERN PS and the 1.1-m^3 heavy-liquid bubble chamber for their indispensable assistance, and our scanning, measuring, and programming staff for their continued efforts over a long period.

[29] N. Cabibbo, in *Proceedings of the Thirteenth International Conference on High-Energy Physics, Berkeley, 1966* (University of California Press, Berkeley, Calif., 1967).

APPENDIX A: NOTATIONS AND SYMBOLS

We denote by τ the decay $K^+\to\pi^+\pi^+\pi^-$ and by τ' the decay $K^+\to\pi^+\pi^0\pi^0$.

p_K = four-momentum of K^+,
$\mathbf{p}_K$ = three-momentum of K^+,
E_K = total energy of K^+,
T_K = kinetic energy of K^+,
m_K = mass of K^+,
} *idem* for π, ν, l^+ (μ^+,e^+).

The square of the four-momentum transferred to the lepton pair is

$q^2=(p_K-p_\pi)^2=(p_l+p_\nu)^2$; in the K^+ rest frame, $q^2=m_K^2+m_\pi^2-2m_KE_\pi$.

$E_\pi'=E_\pi^{\max}-E_\pi$, where $E_\pi^{\max}=(m_K^2+m_\pi^2-m_l^2)/2m_K$ is the maximum pion energy in the K^+ rest frame.

$\mathcal{P}$ = polarization vector for μ^+.

$\hat{\mu}=\mathbf{p}_\mu/|\mathbf{p}_\mu|$,
$\hat{n}=(\mathbf{p}_\pi\times\mathbf{p}_\mu)/|\mathbf{p}_\pi\times\mathbf{p}_\mu|$,
$\hat{t}=\hat{\mu}\times\hat{n}$,
} unit vectors defining a reference frame for a $K_{\mu3}$ event.

$\hat{e}$ = unit vector along emission direction of μ-decay positron,

$\mathcal{P}_L=\mathcal{P}\cdot\hat{\mu}$ = longitudinal polarization of muon,
$\mathcal{P}_T=\mathcal{P}\cdot\hat{t}$ = transverse polarization of muon,
$\mathcal{P}_N=\mathcal{P}\cdot\hat{n}$ = normal polarization of muon.

The coordinates (x,y,z) of space points are given with respect to a right-handed set of axes. The z axes passes along the central axis of the cylindrical chamber, parallel to the mean magnetic field and to the optic axes of the three cameras. The origin is at the glass-liquid interface so that points in the chamber correspond to negative values of z. We define $r=(x^2+y^2)^{1/2}$.

APPENDIX B: $K_{\mu3}$ DECAY KINEMATICS

1. Dalitz-Plot Density

This is obtained from summing over spin states and introducing the kinematical constraints that four-momentum be conserved. In the rest frame of the decaying K^+,

$$\rho=\frac{d^2N}{dE_\pi dE_\mu}\propto A|F_+|^2+B\,\mathrm{Re}(F_+^*F_-)+C|F_-|^2$$
$$=|F_+|^2\{A+B\,\mathrm{Re}\Xi+C|\Xi|^2\},$$

where[30]

$$\Xi=F_-/F_+,$$
$$A=m_K(2E_lE_\nu-m_KE_\pi')+m_l^2(\tfrac{1}{4}E_\pi'-E_\nu),$$
$$B=m_l^2(E_\nu-\tfrac{1}{2}E_\pi'),$$
$$C=\tfrac{1}{4}m_l^2E_\pi'.$$

[30] For pure vector coupling, $\Xi\to\xi=f_-/f_+$.

2. μ^+ Polarization in $K_{\mu 3}^+$

It has been shown[31] that in any decay configuration the μ^+ is completely polarized and that the direction of polarization is uniquely determined by Ξ alone[30]:

$$\mathcal{P}_\mu(\Xi)=\mathbf{A}(\Xi)/|\mathbf{A}(\Xi)|\,,$$

$$\mathbf{A}(\Xi)=a_1(\Xi)\mathbf{p}_\mu-a_2(\Xi)\left\{\mathbf{p}_\pi+\mathbf{p}_\mu\left[\frac{m_K-E_\pi}{m_\mu}+\frac{(\mathbf{p}_\pi\cdot\mathbf{p}_\mu)(E_\mu-m_\mu)}{m_\mu|\mathbf{p}_\mu|^2}\right]\right\}+\mathrm{Im}(\Xi)m_K(\mathbf{p}_\pi\times\mathbf{p}_\mu)\,,$$

with

$$a_1(\Xi)=(m_K^2/m_\mu)[2E_\nu+(\mathrm{Re}\Xi-1)E_\pi']\,,$$
$$a_2(\Xi)=m_K^2+(\mathrm{Re}\Xi-1)m_KE_\mu+\tfrac{1}{4}m_\mu^2(1-2\ \mathrm{Re}\Xi+|\Xi|^2)\,.$$

APPENDIX C: UNCORRELATED PARAMETERS

When q^2 dependence of ξ is described with the parameters $\xi(0)$ and Λ, lines of equal value of the likelihood function—for example, the 1-standard-deviation contour—appear as oblique ellipses in the $[\xi(0),\Lambda]$ frame. These parameters are not independent, and cannot be accurately determined simultaneously; it is thus more useful to express the linear q^2 dependence of ξ in terms of a pair of uncorrelated parameters.

There is an infinity of such pairs; they can be formed from any two linear combinations of $\xi(0)$ and Λ,

$$x_1=a_1\xi(0)+b_1\Lambda=a_1\xi(b_1m_\pi^2/a_1)\,,$$
$$x_2=a_2\xi(0)+b_2\Lambda=a_2\xi(b_2m_\pi^2/a_2)\,,$$

such that the directions $x_1=0$ and $x_2=0$ in the $[\xi(0),\Lambda]$ frame be parallel to a set of conjugated diameters of the ellipses. For simplicity in this analysis, one of the parameters is always taken to be either $\xi(0)$ or the slope

$$\Lambda=\frac{d\xi(q^2)}{d(q^2/m_\pi^2)}\,,$$

and the point $\xi(q_*^2)$ uncorrelated with this parameter is sought. In the first instance, the linear q^2 dependence of $\xi(q^2)$ is parametrized by two points, $\xi(0)$ and $\xi(q_1^2)$, on this line while in the latter it is parametrized by one point $\xi(q_2^2)$ and the slope Λ.

Referring to Fig. 36, q_1^2 and q_2^2 are given by the equations

$$q_i^2/m_\pi^2=-\tan\alpha_i\quad(i=1,2)\,,$$

where $\tan\alpha_i$ are, respectively, the slopes of the conjugated diameters of the ellipse with respect to the $\xi(0)=0$ direction (Λ-axis) and the $\Lambda=0$ direction [$\xi(0)$ axis]. Clearly $\alpha_1\neq\alpha_2$, and thus $q_1^2\neq q_2^2$, but if the ellipse is very elongated, as is always the case in this analysis, then the two values lie very close. This means that $\xi(q_*^2)$, where

$$q_*^2=\tfrac{1}{2}(q_1^2+q_2^2)\,,$$

is almost uncorrelated with both $\xi(0)$ and Λ.

Furthermore, $\xi(q^2)$ is most accurately determined at the point $q^2=q_2^2$, and, if ξ is assumed to be independent of q^2, the value determined is $\bar{\xi}=\xi(q_2^2)$.

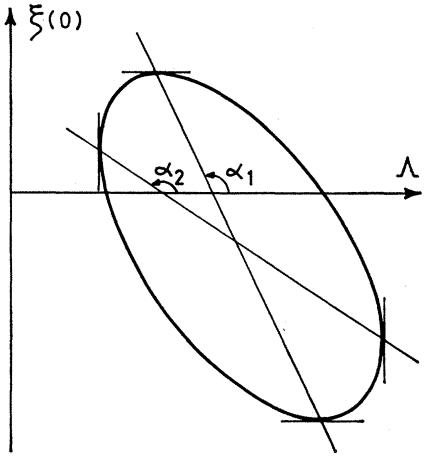

FIG. 36. Geometrical definition of $q_i^2=-\tan\alpha_i$ from an ellipse of equal value of the likelihood function in the frame $[\xi(0),\Lambda]$.

APPENDIX D. COMPUTATION OF ERRORS FROM LIKELIHOOD PLOTS

The following considerations do not depend on whether the parameters are correlated or not, but they assume a Gaussian shape for the likelihood function.

For a one-parameter likelihood analysis, the 1- and 2-standard-deviation limits are obtained by subtraction, respectively, 0.5 and 2.0 from the maximum of the logarithm of the likelihood function.

In a two-parameter analysis, the (-1.14) and (-3.10) contours define the areas inside which the true values of both parameters have, respectively, 68% and 95% probability to lie simultaneously. The uncertainty on one of the parameters, when it is estimated independently of the other, is given by its marginal distribution obtained by integrating over all values of the other variable; this is equivalent to projecting the (-0.5) contour onto the corresponding axis.

When three parameters are estimated, the volumes (in the three-parameter space) inside which the three parameters lie simultaneously with 68% and 95% probability are ellipsoids, the surface of which is defined by subtracting, respectively, 1.8 and 3.9 from the maximum value of the logarithm of the likelihood function. But when each parameter is estimated independently of the two others, the error is obtained by projecting the (-0.5) ellipsoid onto the corresponding axis.

[31] N. Cabibbo and A. Maksymowicz, Phys. Letters 9, 352 (1964).